3. Results and Discussion

3.1. Morphology Analysis and Density Measurements

SEM images of the reinforcement are shown in Figure 1. Figure 1A depicts particles constituting DE used in this study. Figure 1B reveals the morphology of a single diatom frustule characterized by a cylindrical shape with regular openings. The main species within the diatomaceous earth used in the current investigations is *Aulacoseira* sp. This species, found currently in seawaters, feature a zip lock between shells (Figure 1C) and delicate struts reinforcing openings in their frustules (Figure 1D). This locking and struts impart to the frustules' high strength, taking advantage of which was one of the aims of the present study.

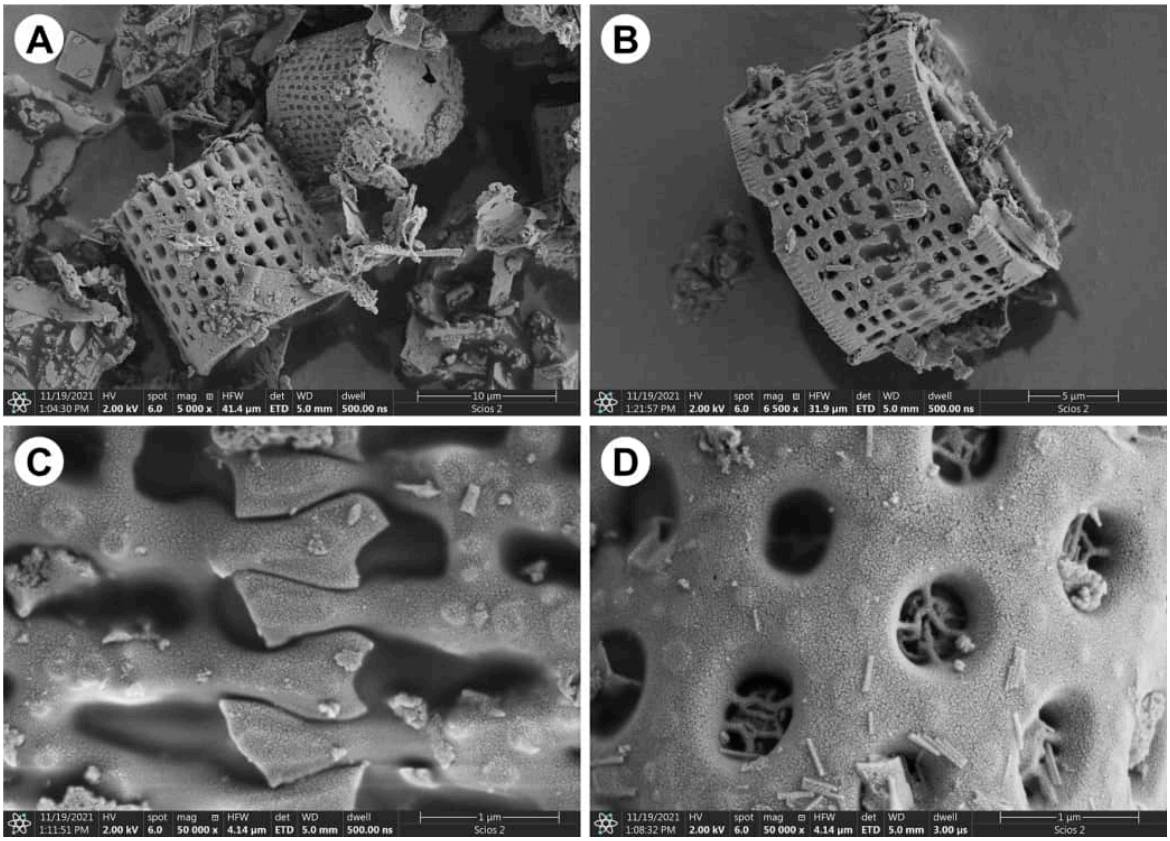

Figure 1. SEM images of the reinforcement—diatomaceous earth: (**A**,**B**) frustules of *Aulacoseira* sp., (**C**) magnification of the zip between frustules, (**D**) magnification of the openings and structures inside the openings.

Representative images of the composites' structure prove fairly uniform distribution of the DE within the polymeric matrix (Figure 2 and Figure S2 in the Supplementary Information). Additionally, penetration of the diatoms' inner cavities by PLA is evidenced.

Results of the measurement of the density of manufactured composites are presented in Figure 3. The results obtained in the measurements of density clearly indicate a considerable porosity, which increases linearly with the content of DE.

Images in Figure 4 reveal two major forms of the pores/voids: (a) delamination between frustules and PLA matrix, (b) unimpregnated cavities of the frustules.

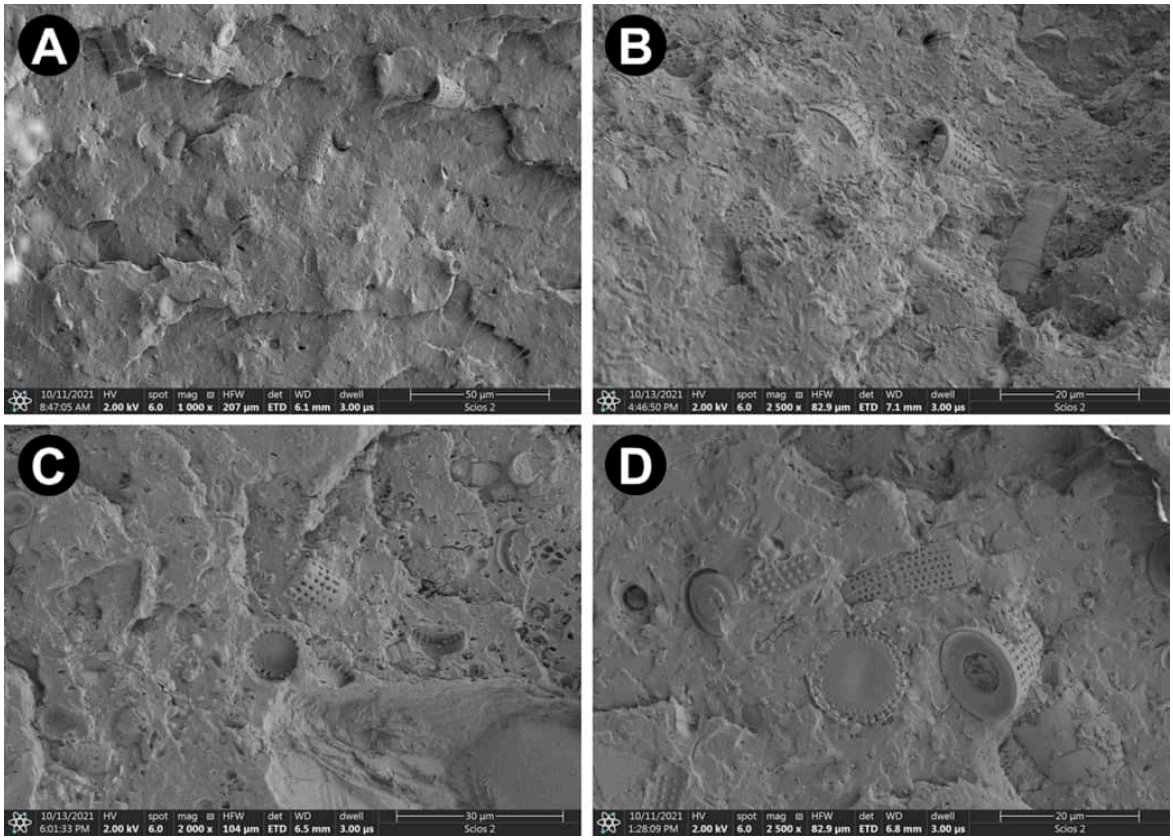

Figure 2. SEM images of the cross-sections of PLA-DE composites showing the uniform distribution of the reinforcement within the polymer matrix (**A**) 2003-5, (**B**) 3001-15, (**C**) 3251-10, (**D**) 4043-10.

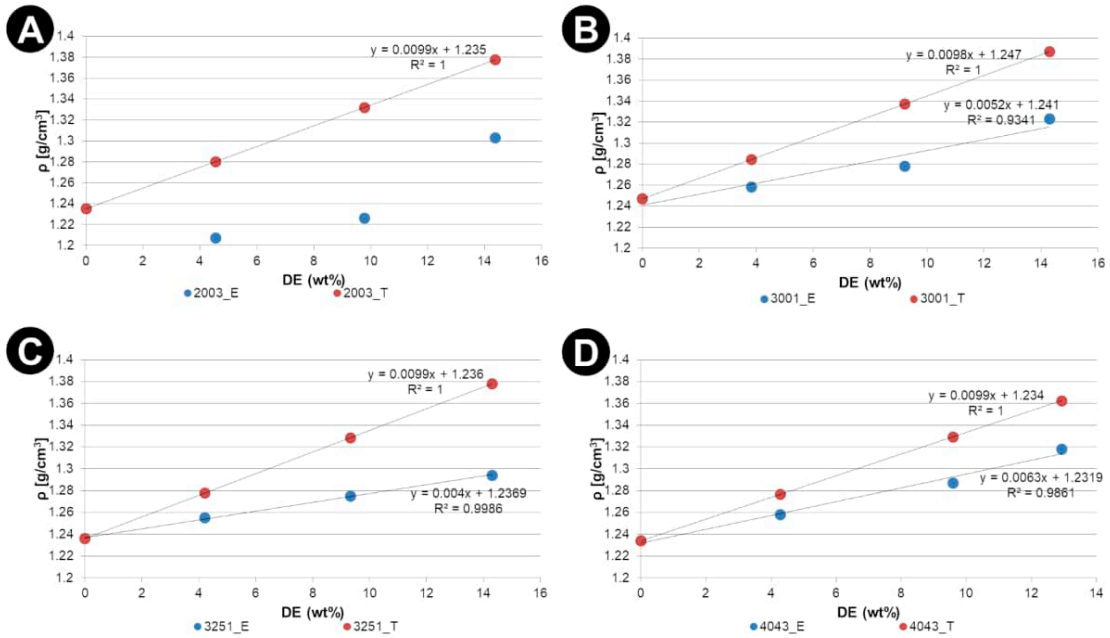

Figure 3. The average density of the manufactured samples against DE weight content in composites with (**A**) 2003D; (**B**) 3001D; (**C**) 3251D and (**D**) 4043D PLA matrices: *E—experimental*, *T—theoretical*.

3.2. Effects of Diatomaceous Earth on the Crystallization of PLA

The effect of DE reinforcement on properties of PLA matrices is demonstrated by the results of DSC test. DSC first heating curves of the composite with the PLA3001D matrix

are shown in Figure 5. Experimental glass transition (T_g), melting temperature (T_m), heat capacity and degree of crystallinity (X_c) are given in Table 2. The DSC first heating curves of other used PLA matrices are presented in the Supplementary Information (see Figure S1).

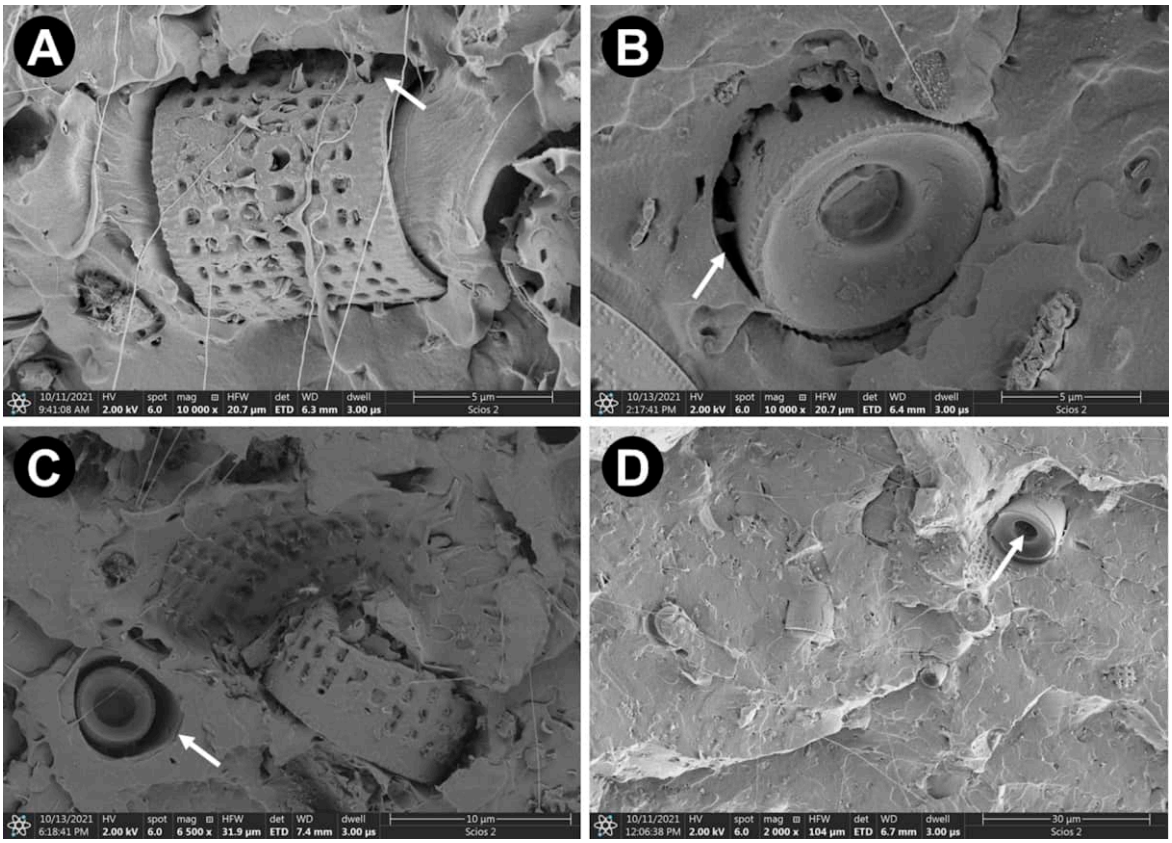

Figure 4. SEM images of the voids (*white arrows*) in manufactured composites: (**A**) 2003-10, (**B**) 3001-5, (**C**) 3251-15, (**D**) 4043-5.

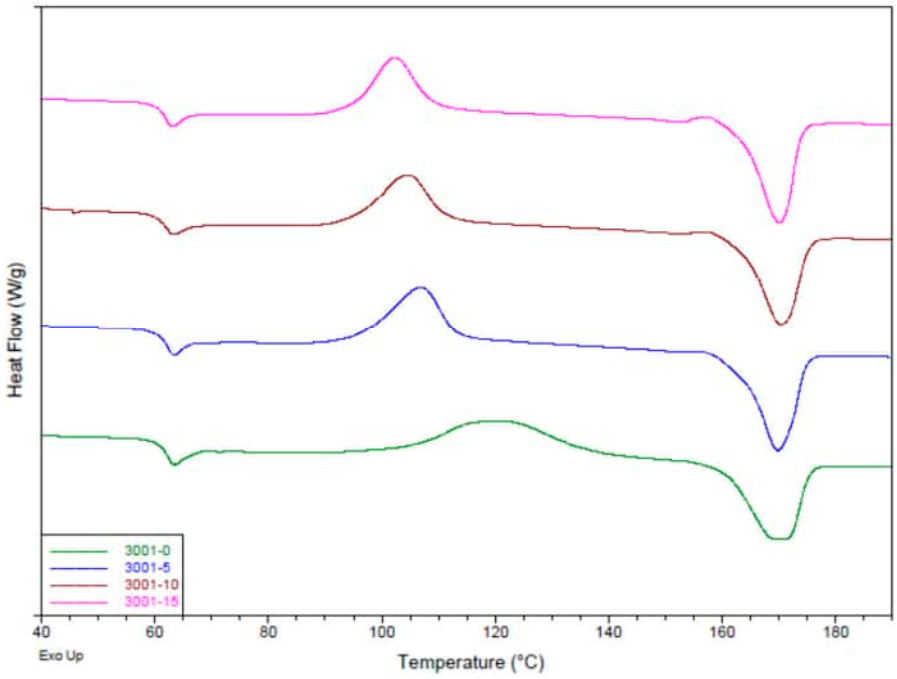

Figure 5. DSC scanning of PLA3001 and 3001 enriched with DE.

Table 2. DSC results for the PLA and the PLA–DE composites.

Sample	T_g [°C]	ΔC_p [J·(g·°C)$^{-1}$]	T_c [°C]	ΔH_c [J·g^{-1}]	T_m [°C]	ΔH_m [J·g^{-1}]	X_c [%]
2003-0	60.7	0.755	119.6	19.26	151.6	21.38	2.28
2003-5	61.1	0.734	125.1	11.35	151.9	15.76	4.97
2003-10	61.1	0.708	121.1	7.16	151.1	13.29	7.30
2003-15	60.9	0.691	117.4	11.06	151.3	17.76	8.41
3001-0	61.9	0.710	121.0	33.34	169.2	41.44	8.69
3001-5	62.3	0.621	107.1	33.09	169.7	41.25	9.10
3001-10	62.2	0.599	104.6	29.69	170.4	37.69	9.45
3001-15	62.1	0.618	102.1	28.56	170.1	37.22	10.84
3251-0	61.7	0.719	107.3	36.46	171.7	44.58	8.75
3251-5	61.6	0.572	103.0	31.77	170.5	41.44	10.88
3251-10	61.4	0.683	102.1	33.11	170.5	45.12	14.28
3251-15	61.7	0.549	101.5	30.20	170.1	40.66	13.16
4043-0	61.5	0.759	122.3	11.90	151.8	16.63	5.09
4043-5	61.3	0.688	126.0	13.56	152.3	18.28	5.30
4043-10	61.4	0.685	123.9	13.50	152.7	18.72	6.21
4043-15	60.9	0.634	122.7	7.99	152.8	14.48	8.01

where (see Section 2.3 Experimental techniques for details): T_g the glass transition temperature; ΔC_p change in the heat capacity; T_c maximum temperature pick of cold crystallization; ΔH_c the cold crystallization enthalpy; T_m the maximum temperature peak of melting; ΔH_m melting enthalpy; X_c the degree of crystallinity.

It can be concluded from DSC tests that addition of DE increased the enthalpy of PLA crystallization phenomena taking place at lower temperatures (*ca*. 107–102 °C), proving the nucleating properties of DE for PLA.

It can be concluded from DSC tests that addition of DE promoted the crystallization phenomena taking place at lower temperatures (*ca*. 107–102 °C), making DE a nucleating agent. Similar phenomenon was observed by Li et al. [6]. This in turn impacts formation of α' crystals, which are favored at temperatures below 110 °C [11]. The disordered α' phase is reported to shift to stable form of α crystals at higher temperatures [12]. As a consequence of its looser chain packing and disordered structure, the α' crystal leads to a lower modulus and barrier properties and to higher elongation at break compared to α crystal [13].

A small exothermic peak can be noticed just before the melting peak at samples 3001-5, 3001-10 and 3001-15. This peak was increasingly visible with the growth of the amount of DE in the material. The most probably it occurred due to the transformation of disordered α' crystals to the ordered α–form [13]. The exothermic peak before melting was visible also in the case of 3251 samples with the addition of DE, whereas the crystallization peak temperature was found to be below 120 °C.

Degree of crystallinity (X_c) calculated from DSC curves increases with the DE content and ranges from 2.28 to 8.41% and from 5.09 to 8.01% for 2003 and 4043, respectively. The observed effect might be a result of the limited molecular mobility, the 2003 and 4043 melting flow index (MFI) is reported by NatureWorks company to be the same, having a value of 6. Low MFI suggests significant resistance, whereas the polymer chain changes its conformation and retards kinetics of the matrix crystallization. At the same time, samples 3001 and 3251 are characterized by an MFI of 22 and 80 (at 210 °C), representatively. Macromolecules can move easier; therefore, the kinetics of crystallization are expected to be higher.

The results obtained indicate also that the addition of DE has no significant impact on the melting point. Significant differences of the melting temperatures are ascribed to the additives of commercial PLA materials. Similarly, no effect on glass transition temperature was found.

3.3. Effects of Diatomaceous Earth Reinforcement on the Mechanical Properties of PLA

The effects of the diatomaceous earth (DE) as mechanical reinforcement are presented in Figures 6–8. The corresponding values of Young's modulus (E), ultimate tensile strength (R_m) and elongation to failure (ε_f) together with the values of the degree of crystallinity have been listed in the Supplementary Information (Table S3).

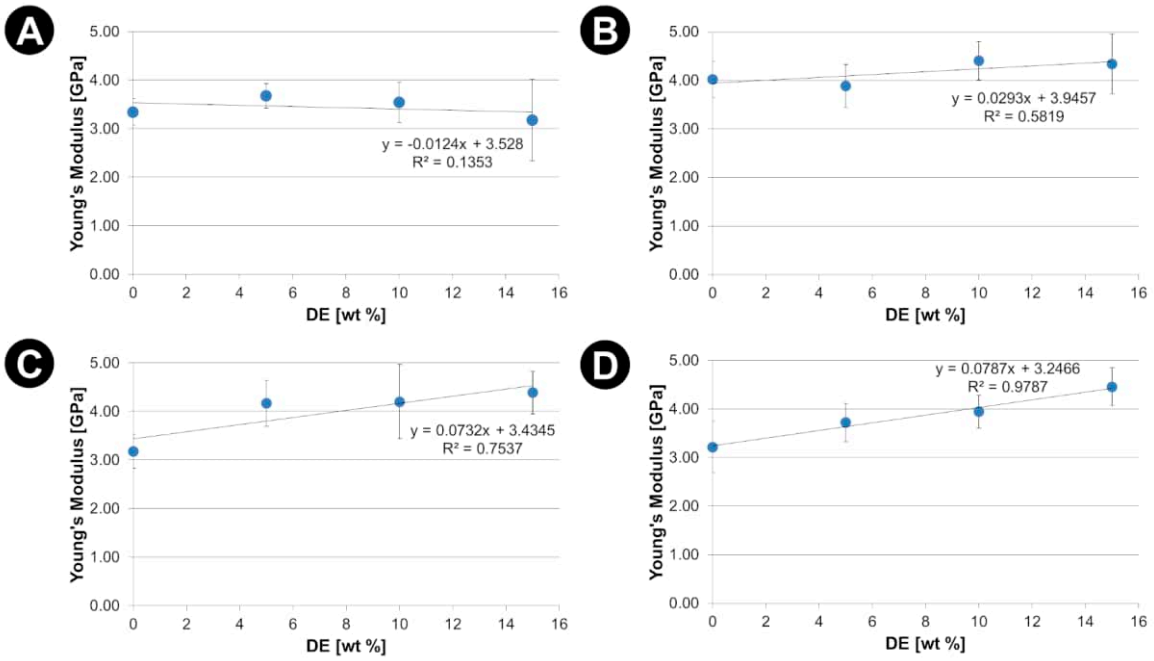

Figure 6. Young's modulus (E) against the DE content for PLA-DE composites with (**A**) 2003D; (**B**) 3001D; (**C**) 3251D and (**D**) 4043D PLA as a matrix.

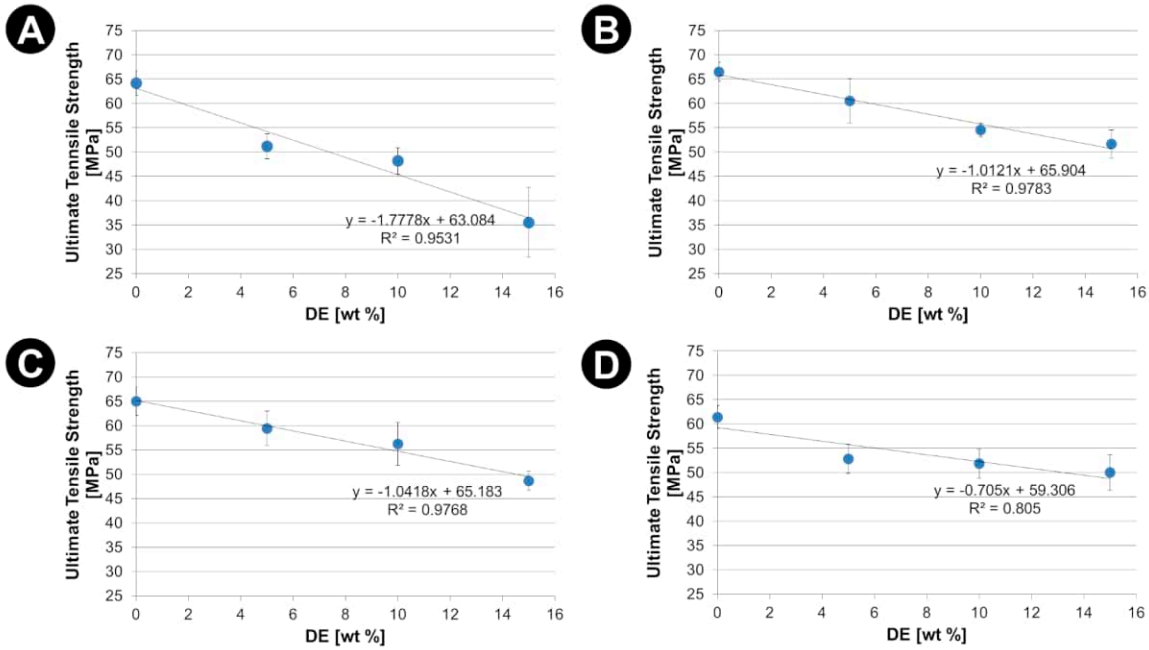

Figure 7. Ultimate tensile strength (R_m) against the DE content for PLA-DE composites with (**A**) 2003D; (**B**) 3001D; (**C**) 3251D and (**D**) 4043D PLA as a matrix.

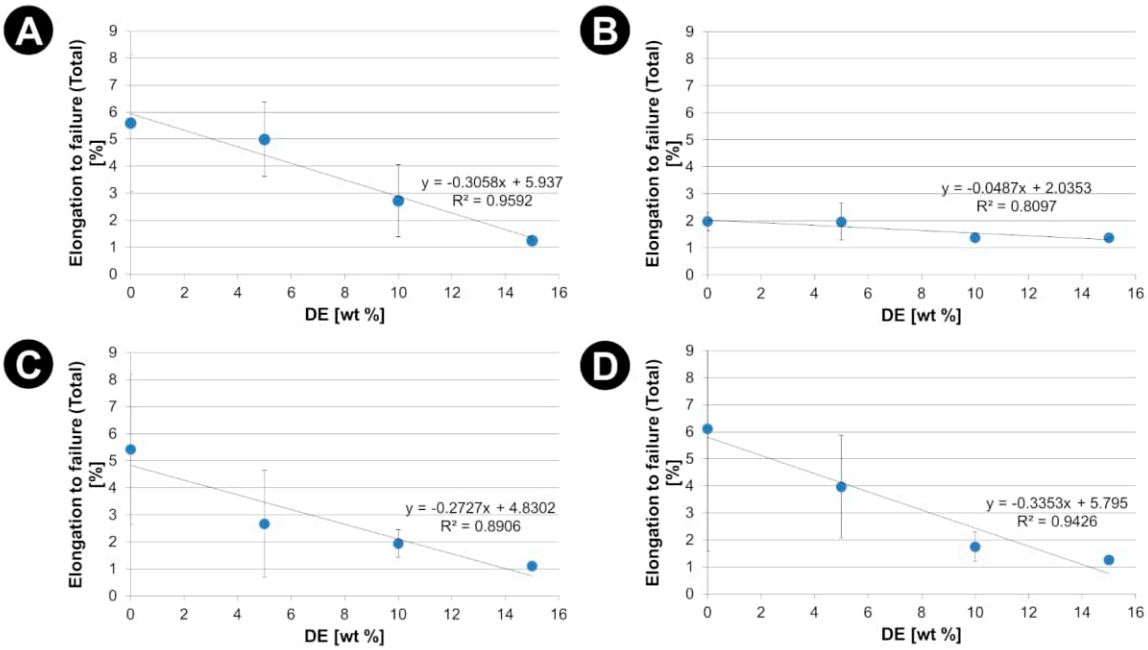

Figure 8. Elongation to failure (ε_f) against the DE content for PLA-DE composites with (**A**) 2003D; (**B**) 3001D; (**C**) 3251D and (**D**) 4043D PLA as a matrix.

For all PLA used in this study with various MFI ratio, a significant increase in the stiffness of the composites (Figure 6) was observed. This can be explained taking into consideration that DE increase in the degree of crystallinity of the manufactured composites. Such mechanism, also observed by Li et al. [6], is experimentally confirmed by the results presented in Supplementary Information (see Table S3). It is also confirmed by SEM observations of breakthroughs of exemplary composites after applying tensile stress within elastic regime, revealing good adhesion between the matrix and reinforcement (Supplementary Information, see Figure S3). Thus, the increase in the stiffness of the manufactured composites can be strictly connected with the morphology of the diatom's frustules. The PLA matrix penetrates to a certain depth into the frustules, which adds value to the adhesion, at least in the range of elastic, reversible stresses, see Figure 9. According to Li et al. [6], such interpenetrating structures may enhance the interfacial interaction, resulting in effective stress transfer and energy dissipation between PLA and DE.

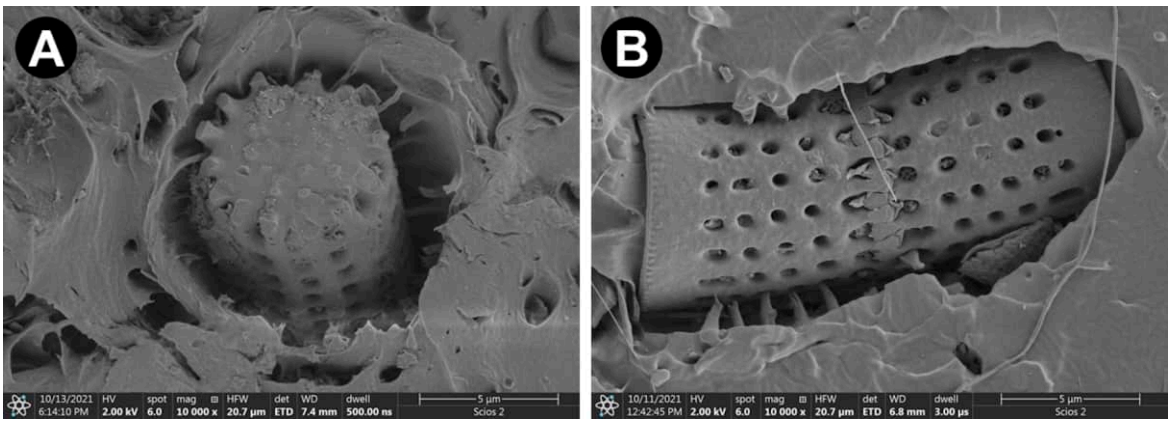

Figure 9. SEM images of the manufactured composites: (**A**) 3251-15, (**B**) 4043-5 showing the created unique structure.

An increase in the crystallinity of the polymer matrix results also in a decrease in its deformation capacity (both elastic and plastic). This effect is confirmed by the significant reduction in the strain to failure (ε_f) with filler content (Figure 8). This effect seems particularly relevant when the material transitions from the elastic to plastic deformation range. With limited adhesion of the matrix to the DE, where adhesion is mediated by the above-mentioned mechanical interlocking of the PLA matrix in the frustule openings, internal de-cohesion of the composite occurs at the onset of plastic deformation.

4. Conclusions

Biodegradable composites in the form of extruded filaments made of various commercial PLA matrices and diatomaceous earth (DE) have been manufactured in a multi-step fabrication process.

The microstructures of the composites revealed uniform dispersion of the reinforcement in the range of 5–15 weight%. During the process of filaments fabrication PLA matrix partially infiltrated into diatom shells. Such partial infiltration results in increased bonding of the matrix to DE frustules by mechanical locking. On the other hand, cavities of frustule which were not fully filled out bring about frustule-originated "caged" porosity, which reduced the specific weight of the composites without reducing their strength. The comparison of true and theoretical density indicates that the porosity is increasing linearly with the content of DE from 1.5 to 8.6%. However, the increase in the porosity does not reduce elastic modulus, which is either maintained or increases with increasing porosity.

Static tensile tests revealed a complex effect of the DE additives on the mechanical properties of composites. Firstly, withing elastic range of strains a noticeable increase in the stiffness of the composites with the addition of DE was observed, which can be attributed to the specific features of diatoms shells. Diatoms shell have a higher stiffness than PLA matrix as their made of bio-SiO_2 and have shape rendering high resistance to compression. On the other hand, a decrease in ultimate tensile strength and elongation to failure was observed. This is related to the composite failure mechanism that occurs once the elastic limit is exceeded. In the plastic deformation case, diatoms can be treated as stress concentrators initiating of progressive destruction of composites. In the current study adhesion of diatoms shells to PLA matrix was primarily due to mechanical locking. We believe that further improving the adhesion of PLA to DEs could increase the ultimate tensile strength of the composites.

DE addition also changes the mechanical properties of the PLA matrix (increase in stiffness, limitation of ultimate tensile strength and elongation to failure) due to the effect of an increased degree of crystallinity. DSC results showed that the DE filler acts as a nucleating agent increasing the degree of crystallinity of the PLA matrices. The crystalline phase increases the stiffness of the matrix but at the same time limits its abilities in large (plastic) deformation, which consequently causes a limitation of ultimate tensile strength.

The conducted investigations showed that biogenic filler in the form of diatomaceous earth can be used as an environmentally friendly additive in biodegradable PLA matrices. Possible applications of these bio-composites are filaments for 3D printing. It should be noted in this context that PLA is one of the most popular filaments used for Fused Deposition Modelling (FDM) printing. The performance of the fabricated filaments in 3D printing is the subject of ongoing investigations.

Supplementary Materials: The following supporting information can be downloaded at: https://www.mdpi.com/article/10.3390/ma15186210/s1, Experimental section: description of true density; Figure S1. DSC scans of the 1st heating of manufactured composites PLA-DE with (A) Ingeo™ Biopolymer 2003D, (B) Ingeo™ Biopolymer 3251D and (C) Ingeo™ Biopolymer 4043D PLA as a matrix; Figure S2. SEM images of breakthroughs of composites with (A–C) PLA2003D, (D–F) PLA3001D, (G–I) PLA3251D, (J–L) PLA4043D matrix and (A,D,G,J) 5 wt% DE, (B,E,H,K) 10 wt% DE and (C,F,I,L) 15 wt% DE reinforcement; Figure S3. SEM images of breakthroughs of composites (A,B) PLA4043D–5 wt% and (C,D) PLA4043D–15 wt% after tensile tests in elastic range; Table S1. The results of the true density; Table S2. The theoretical and experimental composition as well as density

of PLA and PLA–DE composites; Table S3. Tensile results and degree of the crystallinity for the PLAs and the PLA/DE composites.

Author Contributions: I.Z.: Conceptualization, Methodology, Investigation, Writing—original draft, Visualization, Supervision, Project administration, Writing—Review and Editing; M.J.-Y.: Methodology, Investigation, Writing—Review and Editing; R.M.: Methodology, Investigation, Writing—Review and Editing; M.K.: Methodology, Supervision, Project administration, Writing—Review and Editing; A.D.: Investigation; J.W.: Investigation; K.D.: Investigation, Writing—Review and Editing; A.B.: Writing—Review and Editing, Supervision; K.J.K.: Supervision, Project administration. All authors contributed to the general discussion, revision and editing the manuscript. All authors have read and agreed to the published version of the manuscript.

Funding: This research work was funded by the project "Advanced biocomposites for tomorrow's economy BIOG-NET" financed by the Foundation for Polish Science from the European Regional Development Fund within the Intelligent Development Operational Program 2014–2020 (POIR.04.04.00-00-1792/18-00).

Informed Consent Statement: Not applicable.

Data Availability Statement: All data generated or analyzed during this study are included in this published article (and its Supplementary Information Files).

Conflicts of Interest: The authors declare that they have no known competing financial interest or personal relationship that could have appeared to influence the work reported in this paper.

References

1. Shogren, R.; Wood, D.; Orts, W.; Glenn, G. Plant-based materials and transitioning to a circular economy. *Sustain. Prod. Consum.* **2019**, *19*, 194–215. [CrossRef]
2. Murariu, M.; Dubois, P. PLA composites: From production to properties. *Adv. Drug Deliv. Rev.* **2016**, *107*, 17–46. [CrossRef] [PubMed]
3. Topal, E.; Rajendran, H.; Zgłobicka, I.; Gluch, J.; Liao, Z.; Clausner, A.; Kurzydłowski, K.J.; Zschech, E. Numerical and experimental study of the mechanical response of diatom frustules. *Nanomaterials* **2020**, *10*, 222. [CrossRef] [PubMed]
4. Dubicki, A.; Zglobicka, I.; Kurzydłowskı, K.J. Investigation of Energy-Absorbing Properties of a Bio-Inspired Structure. *Metals* **2021**, *11*, 881. [CrossRef]
5. Zglobicka, I.; Jablonska, J.; Suchecki, P.; Mazurkiewicz-Pawlicka, M.; Jaroszewicz, J.; Jastrzebska, A.; Pakiela, Z.; Lewandowska, M.; Swieszkowski, W.; Witkowski, A.; et al. Frustules of Didymosphenia geminata as a modifier of resins. *Inżynieria Mater.* **2018**, *1*, 10–16. [CrossRef]
6. Dobrosielska, M.; Przekop, R.E.; Sztorch, B.; Brzakalski, D.; Zgłobicka, I.; Łępicka, M.; Dobosz, R.; Kurzydłowski, K.J. Biogenic composite filaments based on polylactide and diatomaceous earth for 3D printing. *Materials* **2020**, *13*, 4632. [CrossRef]
7. Dobrosielska, M.; Dobrucka, R.; Brząkalski, D.; Gloc, M.; Rębiś, J.; Głowacka, J.; Kurzydłowski, K.J.; Przekop, R.E. Methodological Aspects of Obtaining and Characterizing Composites Based on Biogenic Diatomaceous Silica and Epoxy Resins. *Materials* **2021**, *14*, 4607. [CrossRef] [PubMed]
8. Li, T.; Sun, H.; Wu, B.; Han, H.; Li, D.; Wang, J.-K.; Zhang, J.; Huang, J.; Sun, D. High-performance polylactic acid composites reinforced by artificially cultured diatom frustules. *Mater. Des.* **2020**, *195*, 109003. [CrossRef]
9. Aguero, A.; Quiles-Carrillo, L.; Jorda-Vilaplana, A.; Fenollar, O.; Montanes, N. Effect of different compatibilizers on environmentally friendly composites from poly(lactic acid) and diatomaceous earth. *Polym. Int.* **2019**, *68*, 893–903. [CrossRef]
10. Gonzalez, L.; Agüero, A.; Quiles-Carrillo, L.; Lascano, D.; Montanes, N. Optimization of the Loading of an Environmentally Friendly Compatibilizer Derived from Linseed Oil in Poly(Lactic Acid)/Diatomaceous Earth Composites. *Materials* **2019**, *12*, 1627. [CrossRef]
11. Aggarwal, S.; Johnson, S.; Saloni, D.; Hakovirta, M. Novel 3D printing filament composite using diatomaceous earth and polylactic acid for materials properties and cost improvement. *Compos. Part B Eng.* **2019**, *177*, 107310. [CrossRef]
12. Singh, B.; Kumar, R.; Singh Chohan, J. Polymer matrix composites in 3D printing: A state of art review. *Mater. Today Proc.* **2020**, *33*, 1562–1567. [CrossRef]
13. Quero, E.; Müller, A.J.; Signori, F.; Coltelli, M.-B.; Bronco, S. Isothermal Cold-Crystallization of PLA/PBAT Blends with and Without the Addition of Acetyl Tributyl Citrate. *Macromol. Chem. Phys.* **2012**, *213*, 36–48. [CrossRef]

Journal Pre-proof

Multi-length scale characterization of frustule showing highly hierarchal structure in the context of understanding their mechanical properties

Izabela Zgłobicka, Krzysztof J. Kurzydłowski

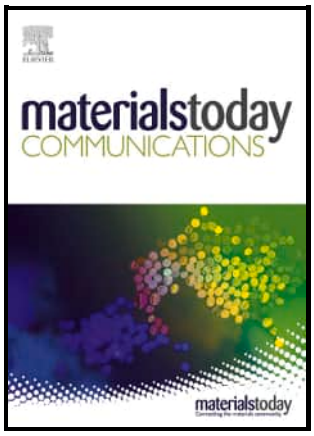

PII: S2352-4928(22)01582-3

DOI: https://doi.org/10.1016/j.mtcomm.2022.104741

Reference: MTCOMM104741

To appear in: *Materials Today Communications*

Received date: 27 July 2022
Revised date: 18 October 2022
Accepted date: 19 October 2022

Please cite this article as: Izabela Zgłobicka and Krzysztof J. Kurzydłowski, Multi-length scale characterization of frustule showing highly hierarchal structure in the context of understanding their mechanical properties, *Materials Today Communications,* (2022) doi:https://doi.org/10.1016/j.mtcomm.2022.104741

Multi-length scale characterization of frustule showing highly hierarchal structure in the context of understanding their mechanical properties

Izabela Zgłobicka[1*], Krzysztof J. Kurzydłowski[1]

[1]Bialystok University of Technology, Faculty of Mechanical Engineering, Wiejska 45C, 15-351 Bialystok, Poland

* i.zglobicka@pb.edu.pl

Abstract

Materials with complex hierarchical structure, called architectured materials or archimats, allow to obtain properties unattainable for their standard form. This paper demonstrates that a multi-length scale imaging is essential for explaining unique properties of such materials/structures, in particular mechanical resilience. Original procedures for multi-scale imaging of biological structures/materials using modern microscopic techniques (electron, ion and X-ray microscopy) are described as applied to an integrated multi-scale description of the diatoms' frustules. The results obtained allowed to advance understanding of their mechanical properties and set the stage for production of advanced structural and functional composite materials.

Keywords

architectured/hierarchical materials, frustules, imaging techniques, properties, bioinspiration

1. Introduction

Properties of standard materials are determined by their chemical compositions and microstructures, the latter being controlled by fabrication technologies. With the variety of technologies available nowadays and large number of well-established ways to select chemical composition, modern materials science offers access to abundance of engineering materials with required mechanical and functional properties. Nevertheless, for some advanced applications there is need to go beyond properties offered by materials already to our disposal. This in particular is likely to happened if high mechanical properties need to be combined with specific characteristics, e.g. light weight. Composites are one of the examples of the ways of increasing the degree of freedom in shaping properties of engineering materials. Over last decades, a number of metal-ceramic composites have been developed for a variety of applications, among others for heat management [1,2]. However, the composites, which by definition are made of dissimilar materials, have some inherent shortcomings related to the interfacial phenomena (such residual stresses, heat and electricity resistance). Also, recycling of devices made of composites is by far more difficult in comparison to one-material solutions.

Thus, a new approach has been recently proposed which is based on the concept of so called architectured materials [3–6], morphology of which imparts functionalities otherwise not achievable. This is possible because of the inner makeup of these architectured materials, or archimats which include composition and internal structure designed at various scale levels. Examples of engineering archimats include periodic cellular or 'lattice' materials, frequently 3D printed, which depending on topology may have unusual mechanical properties, *i.e.,* negative Poisson's ratio [7,8]. It should be noted that complexity of currently designed lattice materials is much reduced in comparison with

living archimats, which acquire special functional properties because of their intricate morphology, as in the case of diatoms [9–13].

Diatom shell, called frustule, are made of bio-silica (SiO_2), a material which hardly can be regarded as offering exceptional properties, both mechanical and physical. On the other hand, it should be reminded that the frustules are grown under conditions limited access to substrates and at ambient temperature. The number of species of these unicellular organisms is estimated in rage of 100 000 – 200 000 [14], whereas the size of the single cell wall is between 2 μm to 5.6 mm [15]. In general, the shell consists of two halves, within which larger overlap smaller, and both are surrounded by several girdle bands.

In the context of architectured materials, diatoms silica frustules show unique, species specific, morphologies in which one can distinguish the features listed in Table 1 and visualized in Figure 1, using example of *Didymosphenia geminata*, *Aulacoseira* sp.

Table 1: The features of diatoms frustules' and properties which they determine

Feature	Length scale	Properties influenced
Frustule box	0.002 to 5.6 mm [15,16]	Resistance to mechanical forces Buoyancy Water flow Superhydrophilicity and superhemophilicity
Frustule's openings	0.064 – 0.5 μm	Gas permeability Light diffraction
Glazing bars	0.049 – 0.095 μm (width)	UV diffraction
Ribs	0.58 ± 0.03 μm (width) 1.25 ± 0.15 μm (height)	Micro and nano-mechanics
Struts	1.05 ± 0.07 μm (length) 0.111 ± 0.31 μm (width)	Micro and nano-mechanics
Pores	ca. 10 nm^2	Specific weight reduction

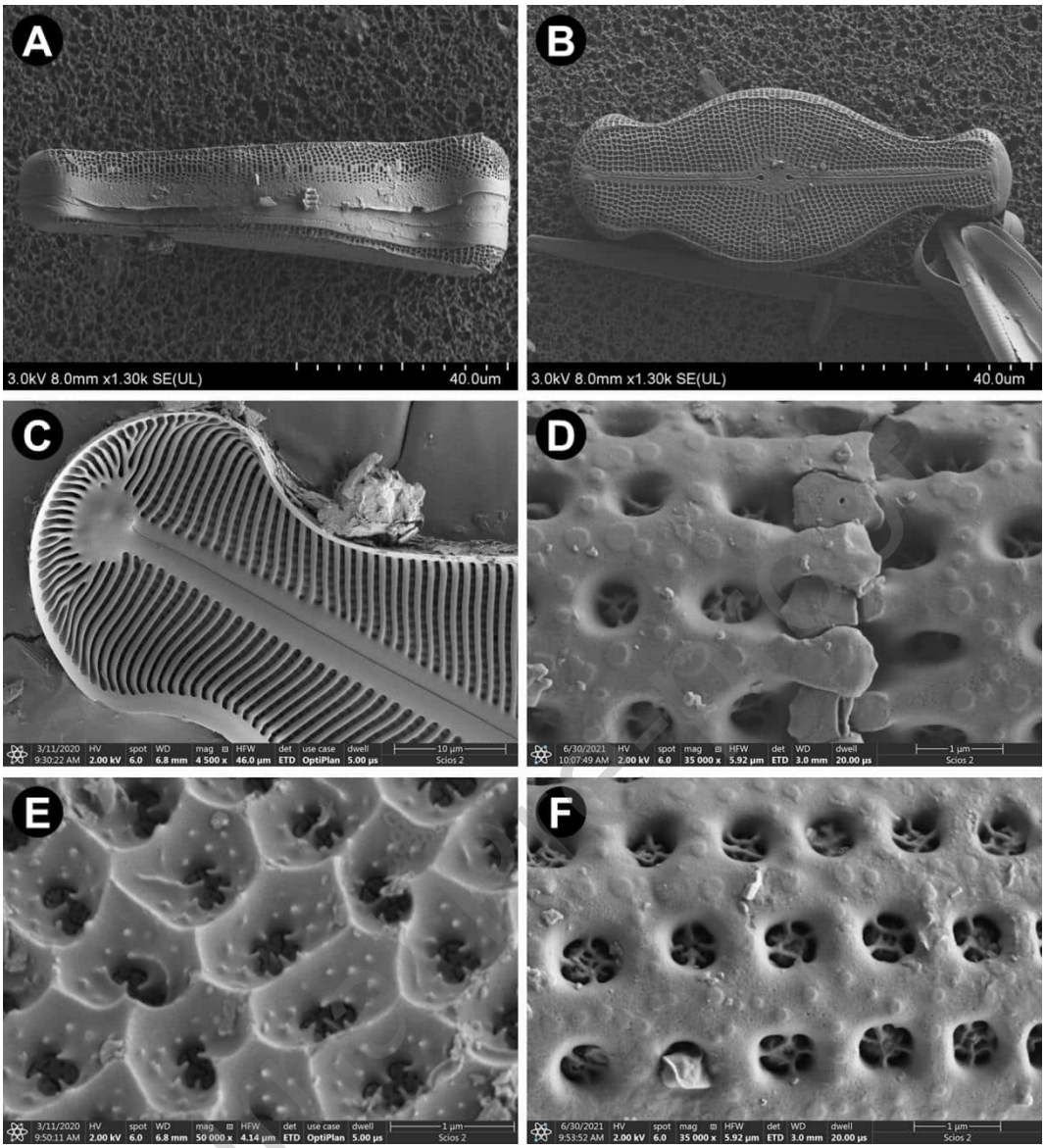

Figure 1: SEM images of diatom frustule (*Didymosphenia geminata* – *DG*; *Aulacoseira* sp. – *AU*) and their characteristic features: (A) girdle band view (*DG*); (B) valve view (*DG*); (C) view of the internal of the frustule – ribs (*DG*); (D) magnification of the connection between frustules (*AU*) (E) magnification of the external valve surface – openings (areaolas) (*DG*), openings with glazing bars (*AU*)

The features listed in Table 1 can be characterized by a number of parameters as listed in Table 2. These parameters can be determined from images of the frustules which, because of the length scale span, require simultaneous use of microscopic techniques, including:

a) light microscopy,
b) scanning electron microscopy,
c) transmission electron microscopy,
d) micro and nano X-ray tomography.

Table 2: Parameters describing the diatoms' frustules and the imaging techniques

Feature	Parameters	Imaging technique
frustule box	length, height	Light microscopy (LM)
	slope angle front and end curvatures	Scanning Electron Microscopy (SEM), X-ray tomography (TXM)
frustules openings	diameter, areal density, lattice constant	Scanning Electron Microscopy (SEM)
glazing bars	thickness, diameter	Scanning Electron Microscopy – Focused Ion Beam (SEM-FIB) X-ray tomography (TXM)
ribs	height, width	
struts	height, width	
pores	diameter, areal density	Transmission Electron Microscopy (TEM), X-ray tomography (TXM)

Due to their structure, among others and nano- to micro-scale porosity of the siliceous diatoms shells can be used in a number of applications, *i.e.,* in filtration processes for molecular and particle separation [9,17,18]. Openings in the shells and their hierarchical structure allow for applications in optics [10,19]. The siliceous cell could be regarded as a 'photonic box' with walls consisting of photonic crystals. In addition, it has been showed that valve of the *Coscinodiscus walessi* focuses an incoming laser light in a small spot of few microns. Recent results reported by Pyia *et al.* [20] show also potential of using diatoms at living templates for fabricating flower-shaped, auto-fluorescent silver-silica (Ag-SiO_2).

Diatoms frustules, also in the form of so called diatomaceous earth, have been also investigated as a biogenic filler in composite materials [21–24]. The preliminary results indicate that the shells increase composite modulus with no specific weight 'penalty'. The frustules have been also considered as a 'caged pores' which reduce the weight of the composite with preservation of its strength far beyond the limitations of the rule of mixing [21] – decoupling of specific weight and strength of the composite [22]. The idea also emerged recently to replicate the intricate morphology of frustules in higher dimensions meta-materials by 3D printing using well established engineering materials such as titanium and polylactide. This new concept has been already presented within several publication in example of titanium shells [25,26].

Highly useful properties of living archimats can only be fully exploited, either directly or indirectly, if precise description of their structure is available. Because of structure complexity the required description need to address all relevant length scale, ranging from nano- to micro-meters. In the present communication, we demonstrate how such description can be obtained with advanced methods of modern materials science, using as an example shell of diatoms obtained from nature (called wild samples) and cultivated within the Szczecin Diatom Culture Collection (SZCZ) (called cultured samples).

2. Experimental procedure

2.1 Material

Described investigations were conducted on diatom frustules obtained from nature (called wild samples) or cultivated within the Szczecin Diatom Culture Collection (SZCZ) (called cultured samples). The preparation procedure included boiling in 37% hydrogen peroxide (H_2O_2) to remove organic matter, rinsing in deionized water and drying in a vacuum dryer at 37°C for 12 h.

2.2 Methods

Light microscopy observations of diatom frustules within aqueous suspension were conducted with a Zeiss Axioscope (Carl Zeiss, Jena, Germany) using phase contrast (PhC) and DIC with a 100x oil immersion objective and Carl Zeiss Axio Imager A2 (Carl Zeiss, Jena, Germany) equipped with Differential Interference Contrast (Nomarski) optics. Images were captured using the Zeiss ICC 5 camera.

For scanning electron microscopy (SEM) observations, the diatom frustules from aqueous suspension were spread over a double-adhesive carbon tape on an aluminum stubs using a pipette and dried. For imaging at highest resolution with field-emission scanning electron microscopy (FE-SEM) samples were coated with conductive (ca. 7 nm) layer (*i.e.,* Au/Pd, Cu/Ni) using Precision Etching Coating System Model 682 (Gatan, Pleasanton, CA, USA). Cross-sectioning and imaging were carried out using dual-beam FIB-SEM tools (Scios2, Thermo Fisher Scientific, USA and Hitachi NB5000, Japan) using acceleration voltages from 2 to 5 kV for the electrons.

The lamella from diatom frustules for transmission electron microscopy (TEM) observations were prepared using a dual-beam FIB-SEM system (Carl Zeiss NVision 40, Carl Zeiss AG, Oberkochen, Germany). The investigation was conducted using a STEM (Carl Zeiss Libra 200 MC Cs, Carl Zeiss AG, Oberkochen, Germany), operating with accelerating voltage of 200 kV to image the nano-structure and nano-porosity.

Scanning transmission X-ray tomography investigations were conducted with a photon energy for Si, range from 1830 to 1890 eV at National Synchrotron Radiation Centre SOLARIS. During experiments, the diatom frustules from aqueous suspension were spread over a TEM grid using pipette and dried. The microscopic images of the raster-scanned sample were obtained by detecting the transmission intensity of the focused X-rays. The spatial resolution of the STXM, typically 20-100 nm, allows to visualize the characteristic for diatom structures, *i.e.,* ribs, areolas. The applied for each region image stack allowed to collect a series of images against the photon energy to obtain a dataset with space (XY) and energy (E) dimensions.

The micromechanical behavior of the *D. geminata* frustule was characterize using microindenter system (Hysitron/Bruker Picoindenter PI87, Brukre/Hysitron, Minneapolis, MN, USA) as a micromanipulator in a DualBeam SEM-FIB system (FEI Helios NanoLab 660, Thermo Fisher Scientific, Waltham, MA, USA). This system allows to conduct in situ indentation experiments on specific locations of the frustule in order to obtain structure response information. A conical indenter with a spherical tip with 3.2 μm was used. The SEM images were recorded during the indentation experiments, and the load versus displacement data were extracted. Indentations have been performed with 1000 and 2000 nm displacement.

Finite element modelling has been carried out using Ansys software (ANSYS Inc., Canonsburg, PA, USA) using geometric models imported from X-ray tomography and refined on the basis of SEM/TEM images. A 3D model of the ribbed surface was built based on the imported geometry. The final mesh consisted of 218 020 finite elements. Pressure of 12.5 Pa and force of 9.5 10^{-5} N were assumed. ANSYS program was used for computations with automatic meshing and under assumption of purely elastic deformation.

3. Results and discussion

3.1 Imaging techniques

Based on light microscopy observations identification of the diatoms date backs to the early 1700s [15]. The first description has been published in 1783 by O. F. Müller [27]. This identification rely on the light microscopy observations which allow to distinguish specific features of different frustules.
Light microscopy is still used to study size and overall shape of the frustules. Recent advances in digital microscopy, including image stacking increased readily available magnifications and depth of focus, allowing for imaging also such details as openings on the valve or girdle band.
It is worth noted, that light microscopy may be used in bright field (BF) and dark field (DF), Figure 2A and Figure 2B respectively. The first one is more common, nevertheless the dark field allows to differentiate topographic surface features on such varied surface as diatom frustule.

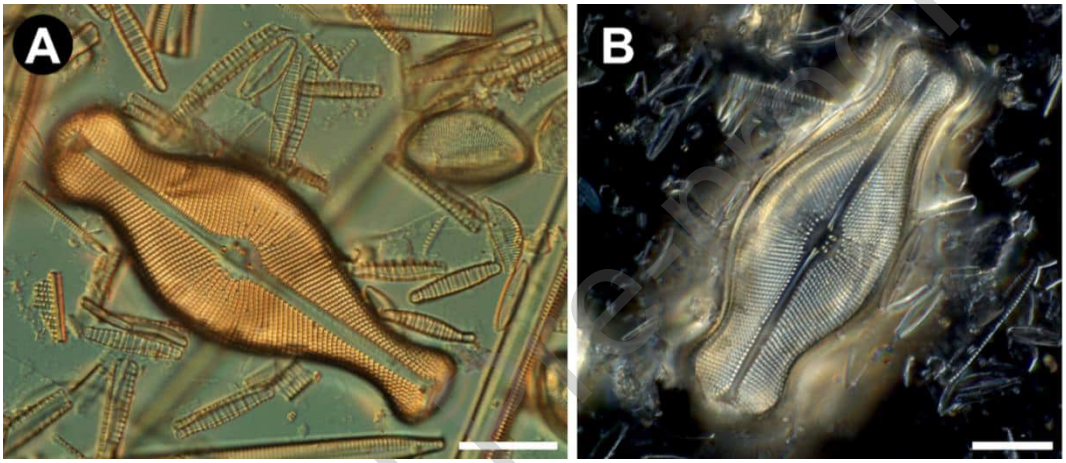

Figure 2: Light microscopy images of *Didymosphenia geminata* frustule in (A) bright field, (B) dark field. Scale bars: 20 µm

Scanning (SEM) images of frustules can be readily obtained with magnification ranging from 100x to 10 000x. This is of particular importance in the case of relatively small species, with frustules size below 50 micrometers. SEM 2D images provide more flexible approach to categorizing of diatoms, which in general either adopt pennate (Figure 3A-E) or centric (Figure 3F, Figure 4A-D) shape. Under higher magnification SEM images reveal fine details of openings in diatoms shells and types of locking between valves, see Figure 4 and Table 3, which depend on their habitat.

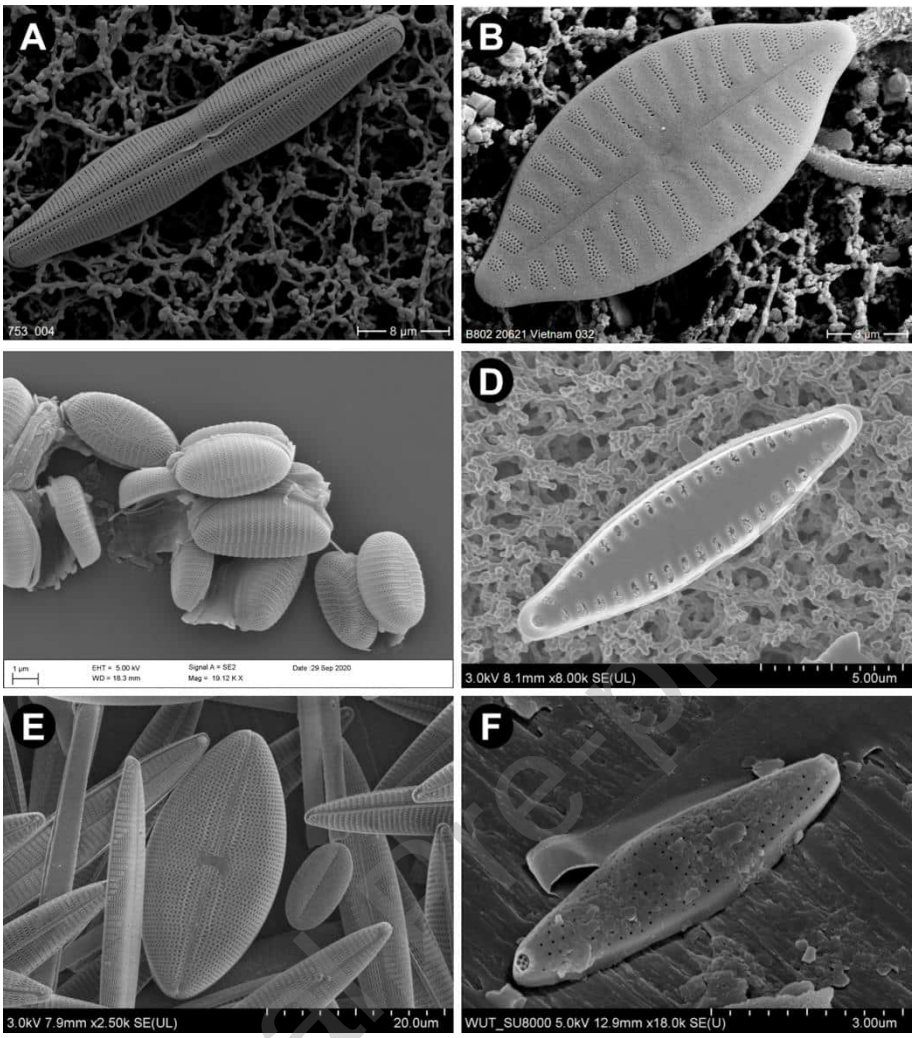

Figure 3: SEM images of diatoms from various habitats: (A) *Craspedostauros* sp., (B) *Planothidium* sp., (C) *Psammoneis obaidii*, (D) *Pseudostaurosira brevistriata*, (E) *Mastogloia* vasta Hustedt, (F) *C. taylorii*

Table 3: Exemplary diatom species from various habitats with their measured characteristic dimensions

No.	Species	Origin	Salinity [‰]	Lenght of the frustule [µm]	Average diameter of the opening [µm]
1.	*Craspedostauros* sp.	Black Sea	35	40.837	0.191±0.020
2.	*Planothidium* sp.	China	7	13.764	0.087±0.008
3.	*Psammoneis obaidii*	Indian Ocean	40	4.936	0.064±0.005
4.	*Pseudostaurosira brevistriata*	Baltic Sea	5	14.203	0.450±0.031
5.	*Mastogloia vasta Hustedt*	Turkey	33.8	31.754	0.309±0.040
6.	*C. taylorii*	South Africa	34.62	6.080	0.065±0.026

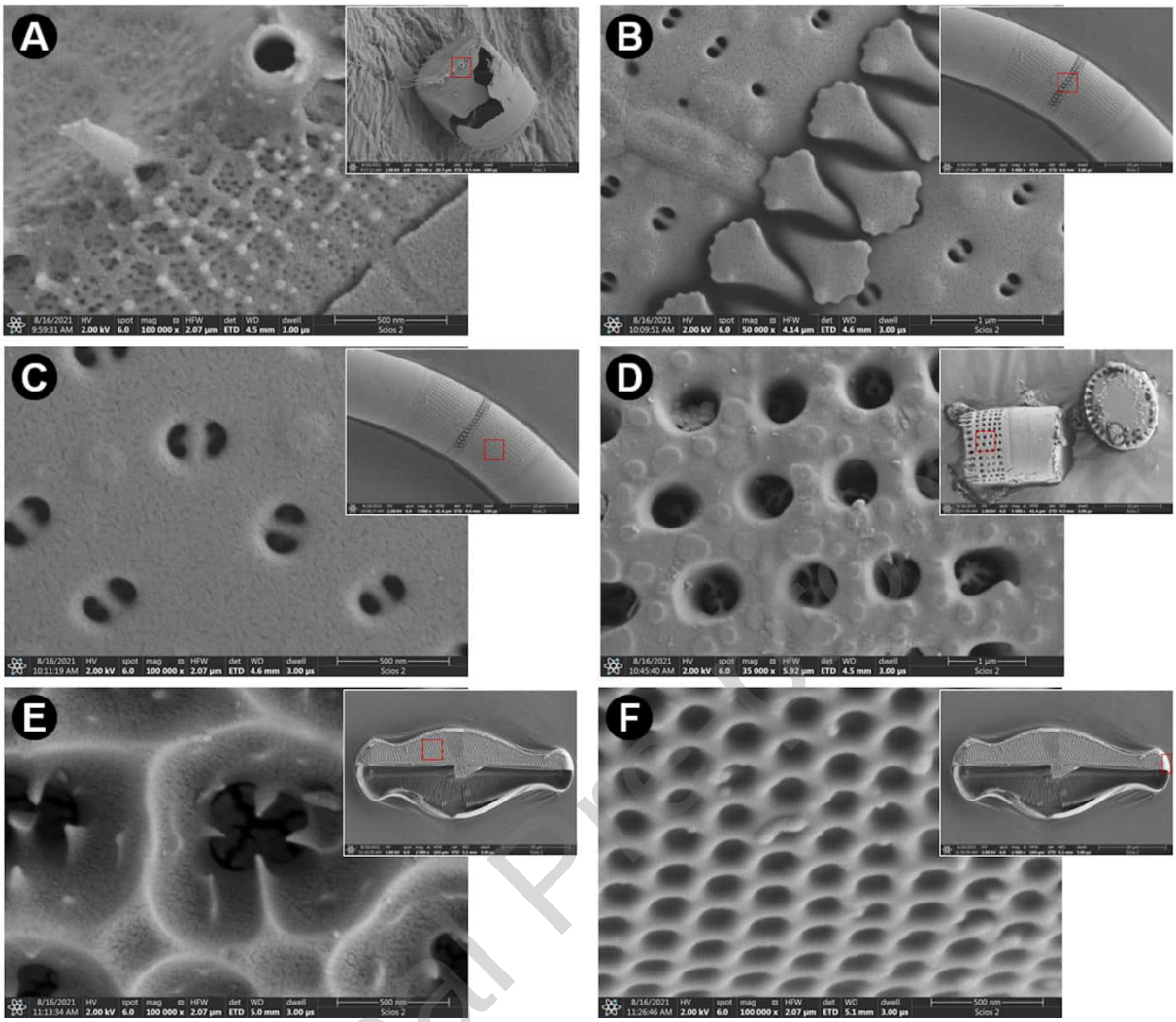

Figure 4: SEM images of characteristic features of (A) *Stephanodiscus parvus* (Biebrza river, Poland) (B-C) *Aulacoseira* cf. *islandica* (Okmin Lake, Poland), (D) *Aulacoseira* sp. (diatomaceous earth, DIATOMIT, Perma Guard), (E-F) *Didymosphenia geminata* (Wisloka river, Poland). Inputs: SEM images of the whole frustules with the designated places of the observations

A new insight into structure of diatoms shells has been offered by instruments offering both imaging with Electron with Ion Beams (SEM+FIB). This is because of possibility of precision sectioning of frustules revealing details of their inner surface. A review recent results obtained with SEM+FIB can be found in Witkowski *et al.* [28]. An example of cross sectioning made to reveal ribbing system of the shell is shown in Figure 5A. As discussed further, such images provide information fundamental to understanding of outstanding mechanical resilience of frustules. In addition, precision cross-sectioning of diatoms frustules (Figure 5A), FIB may be also used for preparation thin samples (Figure 5B) for observations conducted with Transmission Electron Microscopy (TEM).

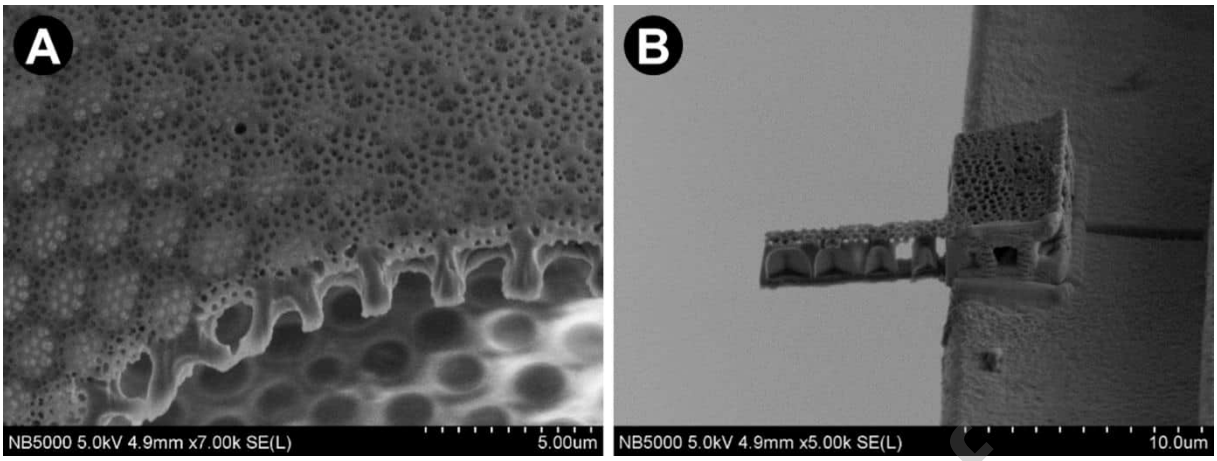

Figure 5: SEM images of the *Coscinodiscus* sp. frustule prepared using dual beam microscope (FIB-SEM): (A) cross-section, (B) lamella

TEM technique requires thin (less than 100 nm thick) samples. On the other hand, imaging with TEM allows for obtaining high resolution images revealing structure of frustules walls and mapping constituent elements, see Figure 6. Meaning of pores and particles revealed in the wall to the biological processes taking place in diatoms is not known yet. Also research on their impact on properties of frustules has only being initiated.

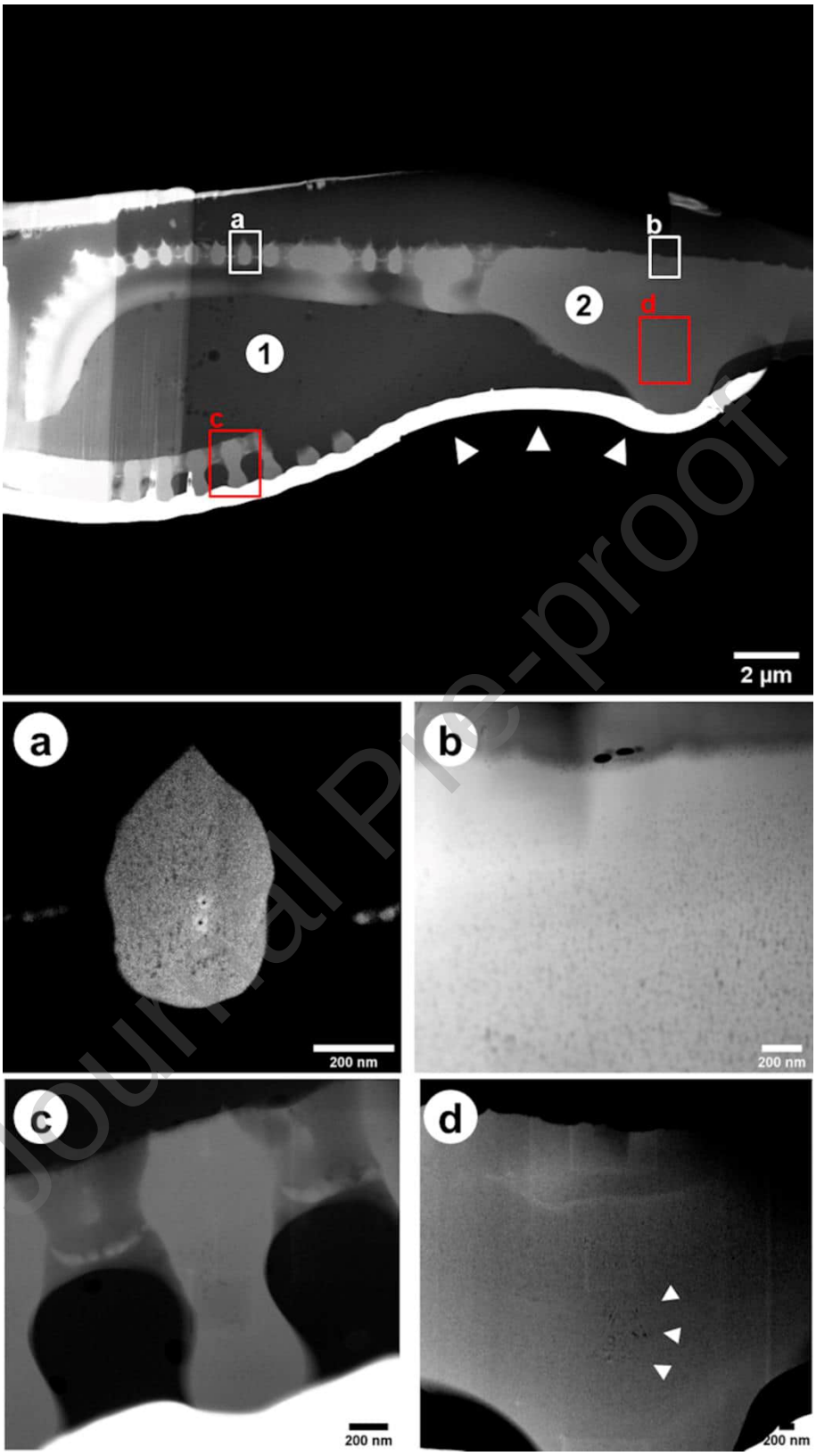

Figure 6: TEM dark field images. Cross-section of *Didymosphenia geminata* frustule: (1) epoxy filling, (2) frustule, white arrowheads: Pt protection layer; (a) single rib with increased contrast to visualize the pores; (b) central area with dense layer on outside; (c) other rib shows also uneven distribution of pores; (d) central area close to stigma with some bigger pores (white arrowheads) (adapted from [21])

X-ray tomography provide a spatial, three-dimensional description of geometry and information on connectivity/curvature/topology of frustules. What is of special importance for testing properties of diatom shell, X-ray tomography can be carried out prior to loading them with mechanical forces and/or fluids. The computed tomography may be realized in several modes within which absorption and phase contrast modes are the most popular. The absorption, X-ray beam passes through the sample and the transmitted radiation is detected to form a simple attenuation contrast image [29]. The phase contrast is used if the material has low-density – attenuation contrast is not sufficient due to the small differences in the attenuation coefficients of materials [29]. It must be noted that investigations using CT imaging may be realized in multiscale – from millimeter resolution to submicron resolution achievable using nano-XCT.

The already conducted investigations on diatoms frustules with nano-XCT revealed fine details of raphe and stigma [30]. Additionally, tomographic data set allows taking a cross-section through any region of the frustule.

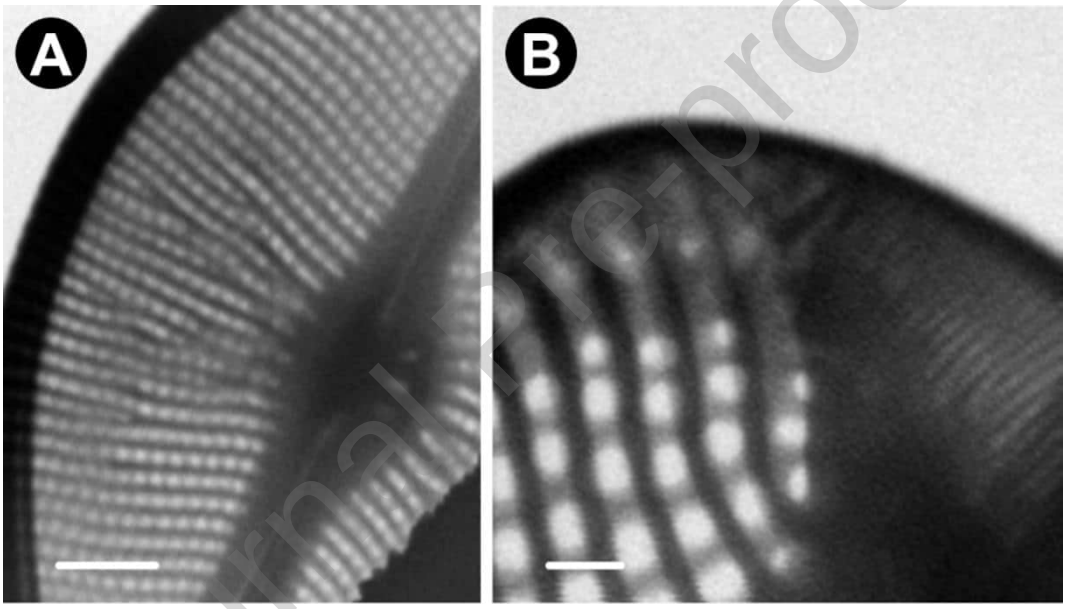

Figure 7: STXM images of *Didymosphenia geminata* frustule: (A) middle part, (B) ending with a pore field. Scale bars: (A) 5 µm, (B) 1 µm

The more accurate X-ray tomography technique, STXM – scanning transmission X–ray tomography, allowed to obtain a microscopic images of the raster-scanned sample by detecting the transmission intensity of the focused X-rays. The high-resolution images because of the length of the whole frustule were possible to obtain only for region of interest (ROI) within the single shell. Therefore, the observations were made sequentially for the endings and the middle part of the shell, see exemplary images on Figure 7. The data from computed tomography can be the input for further investigations like, *i.e.,* computer simulations and 3D models for additive manufacturing [25,26].

Based on the obtained image stacks, the comprehensive analysis of the content of silica in specified regions has been conducted. It must be noted that such results and measurements have been realized for diatom shells for the first time (Figure 8).

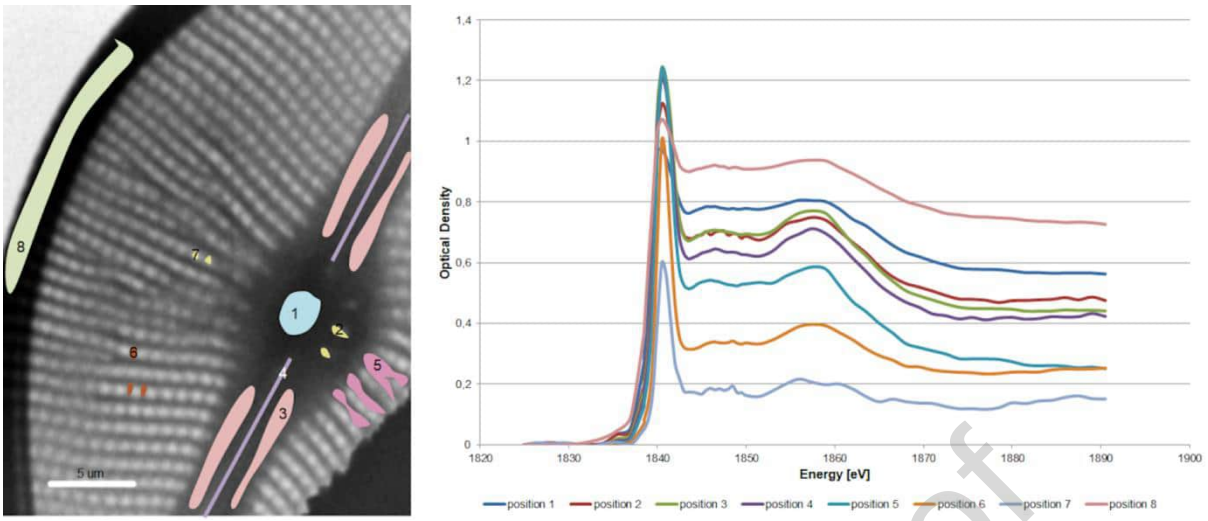

Figure 8: STXM image of the middle part of *D. geminata* frustule with the marked regions and corresponding plot of the optical density (OD) against the photon energy

The region with the highest content of silica is shown in Figure 8 in the border of the frustule, further in the center area of the shell and within the ribs. The exact values of the SiO_2 may be calculated based on the obtained energy spectra. Also, presence of other elements, in addition to Si and O, can be quantitatively determined using this technique.

Results presented in this section provide an example of holistic description of a diatom frustule in the length scales ranging from nano- to micro-meters. This example clearly demonstrates complex and hierarchical character of frustules, which need to be taken into account in modelling their properties and designing applications. Depending on a property in question, different elements of such a holistic description are relevant. For example, mechanical resistance to compression of shall primarily depend on data, which can be extracted from light microscopy images of diatoms. On the other hand, resistance to localized force can only be analyzed based on higher resolution SEM images (analysis of mechanical properties is subject of the next section). On the other hand, X-ray microscopy and high-resolution TEM provide information relevant to functional properties of frustules, in particular photonic. If a basket of required properties includes both mechanical and physical, the approach adopted here sets the stage for such advanced applications of diatoms frustules.

3.2 Mechanical properties

The main component of the diatoms' frustules is silica, one of the most complex and most abundant materials, existing as a compound of several minerals but also as a synthetic product. It is known that silica (silicon dioxide, SiO_2) is not material of remarkable mechanical properties (see Table 4). Modulus of elasticity is in the range of 71.2 – 74.8 GPa. Because of a low density – 2.2 g/cm^3 – specific modulus of silica is similar to that of engineering composites or alloys [31].

Table 4: The comparison of physicochemical properties of synthetic and biogenic silica (data for diatomaceous earth has been designated with *)

No.	Property	Synthetic silica (SiO_2)	Biogenic silica (diatoms frustules / diatomaceous earth)
1.	Density	2.650 g/cm^3	2.274 g/cm^3
2.	Compressive strength	1100 – 1600 MPa	7.67 MPa [32] 330-680 MPa [33]
3.	Hardness	4.5-9.5 MPa	1-12 GPa [34,35]
4.	Modulus of rupture	110-200 MPa	*no data available*
5.	Poisson's ratio	0.15-0.19	*no data available*
6.	Shear modulus	27.9-32.3 GPa	*no data available*
7.	Tensile strength	45-155 MPa	155 – 560 MPa [33] girdle bands: 155 MPa costae: 560 MPa
8.	Young's modulus	66.3-74.8 GPa	7 – hundreds GPa [34,35] transapical rib: 7-20 GPa central rib: 15-100 GPa central nodule: 30 – hundreds GPa 22.4 GPa [33]
9.	Glass temperature	1230-1830 K	*no data available*
10.	Specific heat	680-730 J/kg*K	*no data available*
11.	Thermal conductivity	1.3-1.5 W/m*K	*no data available*
13.	Thermal expansion	0.55-0.75 10^{-6}/K	*no data available*

Special, complex architecture of silica frustules results in their mechanical properties exceeding properties of a simple-shaped dense lump of silica. High strength and resilience of silica frustules, *i.e.,* crush resistance [33] can be explained by analyzing results of micro- and nano-indentation tests [34,36,37].

Of special interest are the results of micromechanical characterization of the diatom frustule via *in situ* SEM indentation. SEM images recorded during indentation tests allowed to conduct comparison of properties/behavior of various regions on diatom frustules. Three main places of the shell have been chosen: (a) valve with complex morphology; (b) dense middle part of the frustule; (c) raphe in the distal end of the frustule. The obtained load-displacements curves for each micro-indentation spots are presented in Figure 9. The micro-indentation experiments revealed that central part of the frustule, which is solid, is characterized by higher values, see Figure 9.

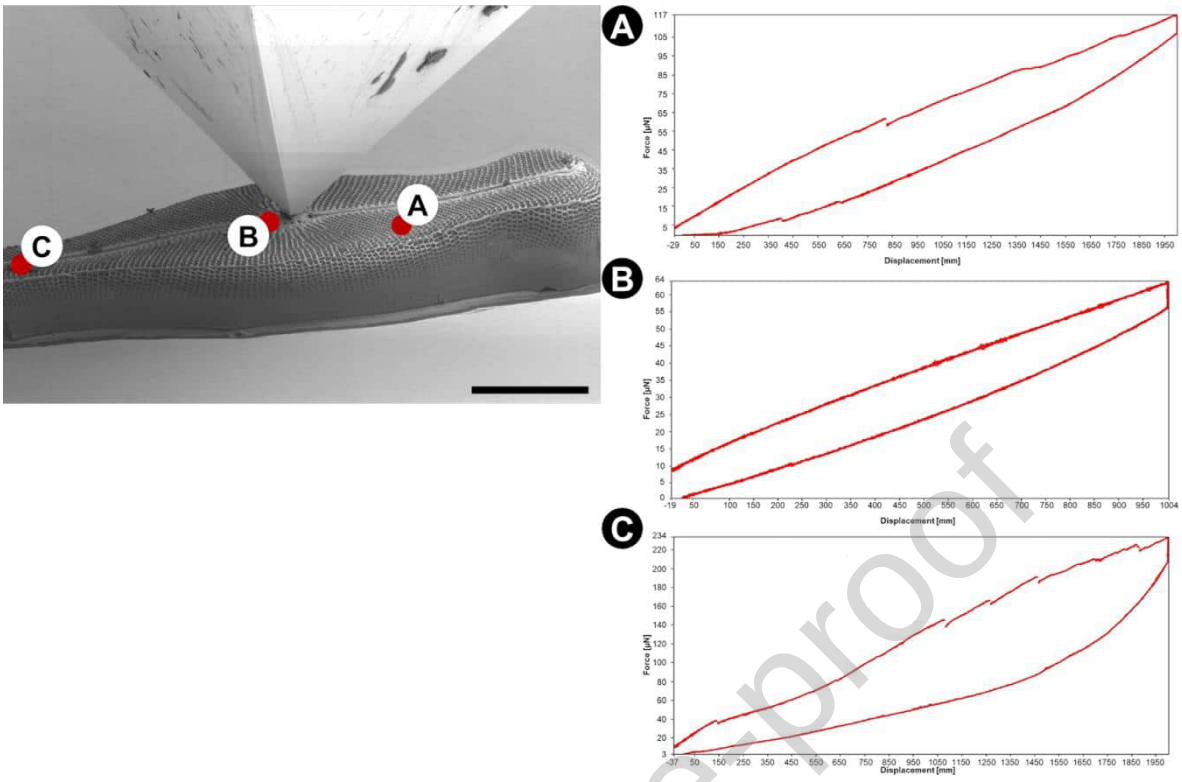

Figure 9: SEM image during in situ indentation with marked places of investigations. Indentations have been performed with (a) 2000 nm, (b) 1000 nm, (c) 2000 nm displacement

Importance of detailed high-resolution description of geometry to understanding of mechanical properties of frustules can be demonstrated by modelling their reaction to mechanical loading by pressure and localized force. These two types of loading are typical of diatoms natural habitat. Pressure is exerted by water and localized force by predators. For both types of loads, ribbed structure of frustules is a key factor, as supported by results of Finite Element Modelling (FEM). Two models (Figure 10) have been prepared, which capture essentials of ribbed-geometry and used to conduct computer simulations. Pressure of 12.5 Pa and force of 9.5 10^{-5} N were assumed. Span and cross-section of ribs were assumed according to the results obtained in FIB-SEM imaging. ANSYS program was used for computations with automatic meshing and under assumption of purely elastic deformation. Mechanical properties of bio-silica were adopted as in given Table 4. Results of FE analysis are illustrated in Figure 11 and 12.

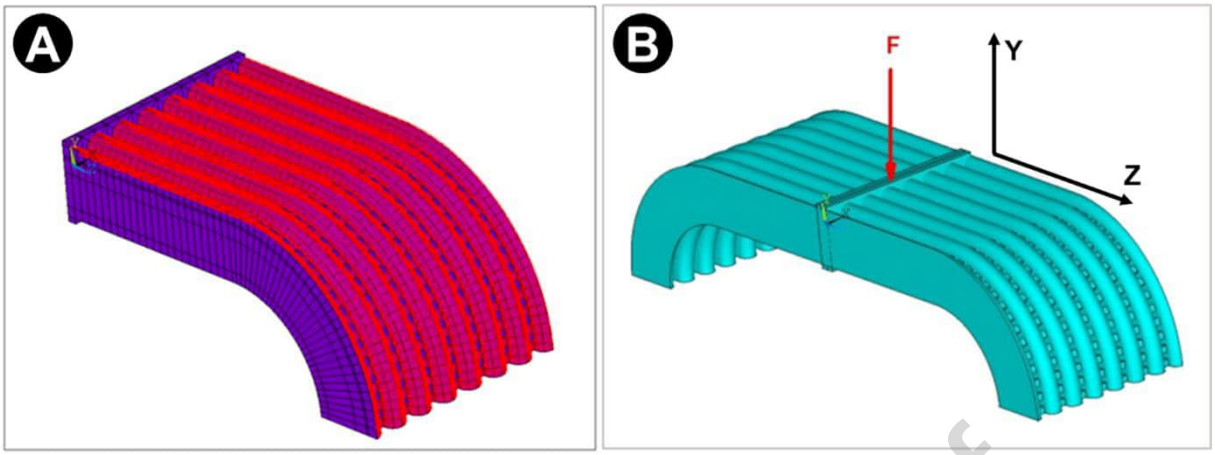

Figure 10: Models of the part of diatom frustule: (A) pressure applied on the upper surface of the structure

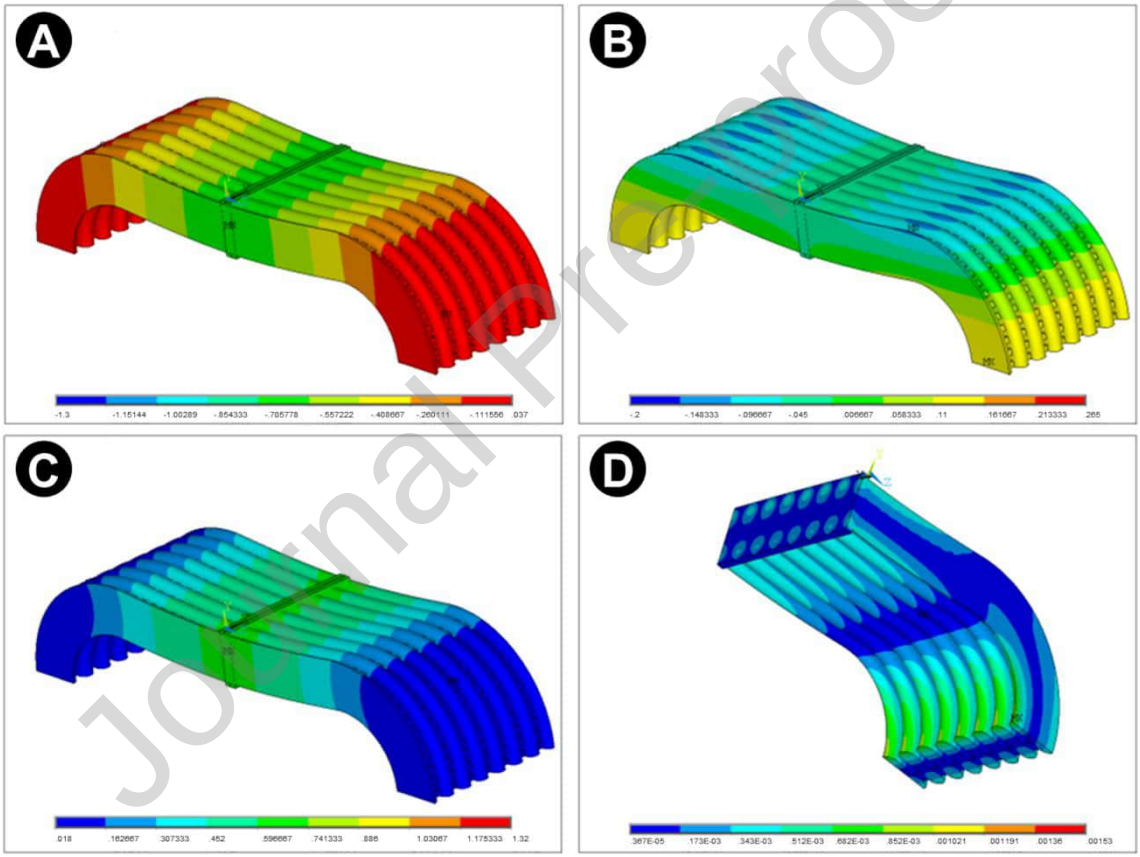

Figure 11: Maps obtained for the pressure applied on the upper surface: (A) displacement in Y direction [µm], (B) displacement in Z direction [µm] (C) accidental displacement and (D) reduced stresses

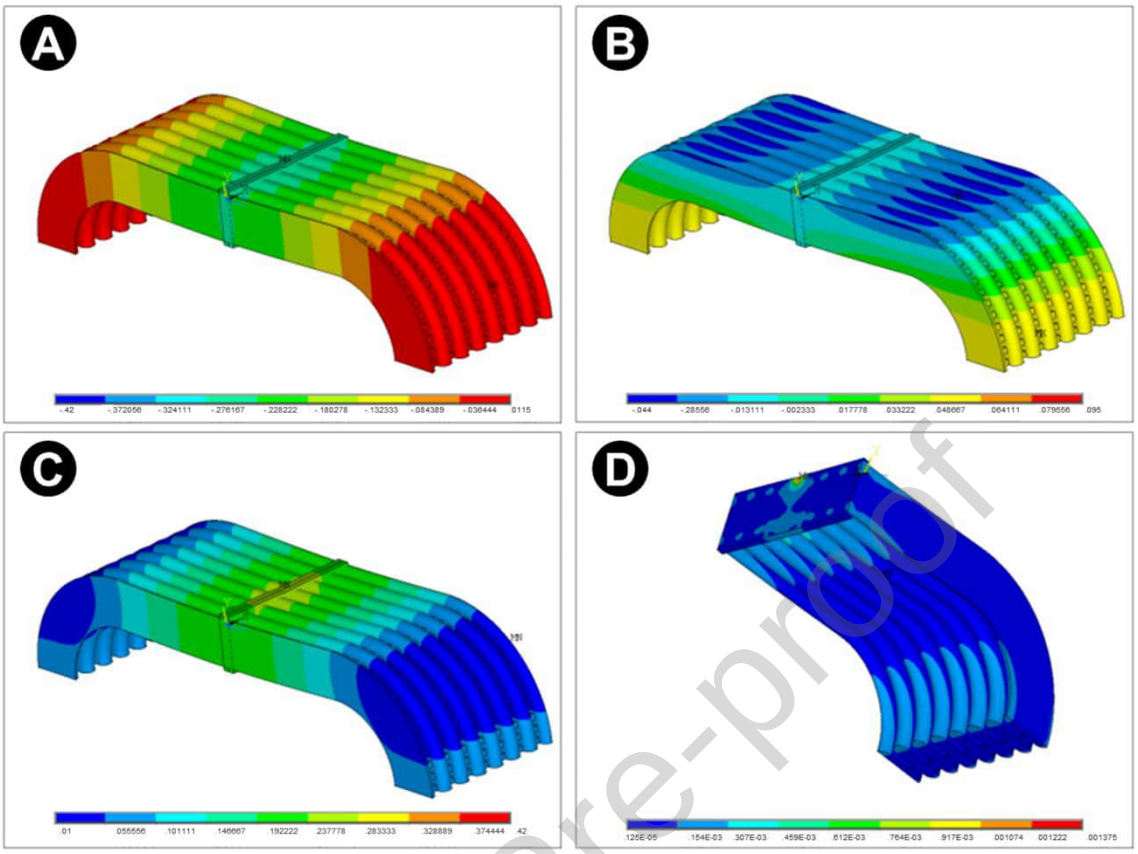

Figure 12: Maps obtained for the force applied on the upper surface: (A) displacement in Y direction [µm], (B) displacement in Z direction [µm] (C) axial displacement and (D) reduced stresses

The obtained results clearly show that the deflection of the shell under pressure and localized force is generally low and concentrates in the central part (along raphe). Such a reaction to these loads, because of mechanical locking along raphe, impart high resilience of frustules to loads experience in their habitat. These results can also be used for bio-mimicking resilient and crush resistant structure, in particular obtained by 3D printing [25].

3. CONCLUSIONS

We presented a comprehensive approach to the characterization of highly hierarchical diatoms' frustules in the context of explaining their unique properties. The methodology adopted here provided a comprehensive description with in the length scale spanning from fraction of millimetres to fraction of micrometres.

A particularly important benefit of using adopted approach is the acquisition of hitherto unavailable information about the details of the structure of diatom shells, including interior, cross-section, but also details of silica walls in nanoscale. These studies allowed to obtain complete topology of the shells, which is important in the context of their mechanical properties but also possible applications.

It has been shown that specific features of various diatoms' frustules, such as regular pattern of openings, struts, ribs imparts high stiffness and resistance to localized forces under reduced mass/weight of the entire structure.

ACKNOWLEDGEMENTS

The authors thank Prof. Andrzej Witkowski, Prof. Ehrenfried Zschech, Dr hab. Teresa Noga, Dr inż. Romuald Dobosz, Dr inż. Tomasz Plocinski, Dr inż. Magdalena Płocińska, Dr Jürgen Gluch, Dr Zhongquan Liao, Dr inż. Bartlomiej Wysocki, Dr Agnieszka Chmielewska, Dr Przemyslaw Dabek, Dr Barbara Wolanin, Dr Krzysztof Matlak, Harishankaran Rajendran, Łukasz Peszek for support in conducted investigations.
Dr Izabela Zgłobicka acknowledges funding provided by German Academic Exchange Service (DAAD) within Research Grants – Short-Term Grants 2017 (ID: 57314023), National Science Center for providing financial support to project Metal Matrix Composites with natural filler (Grant No. 2018/31/D/ST8/00890) and National Synchrotron Radiation Centre SOLARIS in Cracow (proposal no. 211029).

CRediT AUTHOR STATEMENT

Izabela Zglobicka: Conceptualization, Methodology, Investigation, Resources, Data Curation, Writing, Visualization, Project administration; **Krzysztof J. Kurzydlowski:** Conceptualization, Methodology, Writing – Review & Editing

DATA AVAILABILITY

All data generated or analyzed during this study are included in this published article.

ADDITIONAL INFORMATION

The authors declare that they have no known competing financial interests or personal relationships that could have appeared to influence the work reported in this paper.

4. REFERENCES

[1] J. Han, G. Du, W. Gao, H. Bai, An Anisotropically High Thermal Conductive Boron Nitride/Epoxy Composite Based on Nacre-Mimetic 3D Network, Adv. Funct. Mater. 29 (2019) 1–9. https://doi.org/10.1002/adfm.201900412.

[2] Y. Shi, C. Wang, Y. Yin, Y. Li, Y. Xing, J. Song, Functional Soft Composites As Thermal Protecting Substrates for Wearable Electronics, Adv. Funct. Mater. 29 (2019) 1–8. https://doi.org/10.1002/adfm.201905470.

[3] M. Ashby, Designing architectured materials, Scr. Mater. 68 (2013) 4–7. https://doi.org/10.1016/j.scriptamat.2012.04.033.

[4] F. Barthelat, Architectured materials in engineering and biology: Fabrication, structure, mechanics and performance, Int. Mater. Rev. 60 (2015) 413–430. https://doi.org/10.1179/1743280415Y.0000000008.

[5] Y. Estrin, Y. Beygelzimer, R. Kulagin, Design of Architectured Materials Based on Mechanically Driven Structural and Compositional Patterning, Adv. Eng. Mater. 21 (2019) 1–12. https://doi.org/10.1002/adem.201900487.

[6] Y. Mao, Q. He, X. Zhao, Designing complex architectured materials with generative adversarial networks, Sci. Adv. 6 (2020). https://doi.org/10.1126/sciadv.aaz4169.

[7] N.A. Fleck, V.S. Deshpande, M.F. Ashby, Micro-architectured materials: Past, present and future, Proc. R. Soc. A Math. Phys. Eng. Sci. 466 (2010) 2495–2516. https://doi.org/10.1098/rspa.2010.0215.

[8] R. Lakes, Advances in negative Poisson's ratio materials, Adv. Mater. 5 (1993) 293–296. https://doi.org/10.1002/adma.19930050416.

[9] J. Parkinson, R. Gordon, Beyond micromachining: The potential of diatoms, Trends Biotechnol. 17 (1999) 190–196. https://doi.org/10.1016/S0167-7799(99)01321-9.

[10] T. Fuhrmann, S. Landwehr, M. El Rharbl-Kucki, M. Sumper, Diatoms as living photonic crystals, Appl. Phys. B Lasers Opt. 78 (2004) 257–260. https://doi.org/10.1007/s00340-004-1419-4.
[11] P.J. Lopez, J. Desclés, A.E. Allen, C. Bowler, Prospects in diatom research, Curr. Opin. Biotechnol. 16 (2005) 180–186. https://doi.org/10.1016/j.copbio.2005.02.002.
[12] J.E.N. Dolatabadi, M. de la Guardia, Applications of diatoms and silica nanotechnology in biosensing, drug and gene delivery, and formation of complex metal nanostructures, TrAC - Trends Anal. Chem. 30 (2011) 1538–1548. https://doi.org/10.1016/j.trac.2011.04.015.
[13] M.S. Aw, S. Simovic, Y. Yu, J. Addai-Mensah, D. Losic, Porous silica microshells from diatoms as biocarrier for drug delivery applications, Powder Technol. 223 (2012) 52–58. https://doi.org/10.1016/j.powtec.2011.04.023.
[14] E.V. Armbrust, The life of diatoms in the world's oceans, Nature. 459 (2009) 185–192. https://doi.org/10.1038/nature08057.
[15] F. Round, R. Crawford, D. Mann, The diatoms. Biology and morphology of the genera, Cambridge University Press, 1990.
[16] R. Gordon, D. Losic, M.A. Tiffany, S.S. Nagy, F.A.S. Sterrenburg, The Glass Menagerie: diatoms for novel applications in nanotechnology, Trends Biotechnol. 27 (2009) 116–127. https://doi.org/10.1016/j.tibtech.2008.11.003.
[17] F. Xu, Y. Wang, X. Wang, Y. Zhang, Y. Tang, P. Yang, A Novel Hierarchical Nanozeolite Composite as Sorbent for Protein Separation in Immobilized Metal-Ion Affinity Chromatography, Adv. Mater. 15 (2003) 1751–1753. https://doi.org/10.1002/adma.200305287.
[18] D. Losic, G. Rosengarten, J.G. Mitchell, N.H. Voelcker, Pore architecture of diatom frustules: Potential nanostructured membranes for molecular and particle separations, J. Nanosci. Nanotechnol. 6 (2006) 982–989. https://doi.org/10.1166/jnn.2006.174.
[19] L. De Stefano, I. Rea, I. Rendina, M. De Stefano, L. Moretti, Lensless light focusing with the centric marine diatom Coscinodiscus walesii, Opt. Express. 15 (2007) 18082. https://doi.org/10.1364/oe.15.018082.
[20] P. Roychoudhury, A. Golubeva, P. Dąbek, M. Gloc, R. Dobrucka, K. Kurzydłowski, A. Witkowski, Diatom Mediated Production of Fluorescent Flower Shaped Silver-Silica Nanohybrid, Materials (Basel). 14 (2021) 7284. https://doi.org/10.3390/ma14237284.
[21] I. Zglobicka, J. Jablonska, P. Suchecki, M. Mazurkiewicz-Pawlicka, J. Jaroszewicz, A. Jastrzebska, Z. Pakiela, M. Lewandowska, W. Swieszkowski, A. Witkowski, K.J. Kurzydlowski, Frustules of Didymosphenia geminata as a modifier of resins, Inżynieria Mater. 1 (2018) 10–16. https://doi.org/10.15199/28.2018.5.2.
[22] M. Dobrosielska, R.E. Przekop, B. Sztorch, D. Brzakalski¸, I. Zgłobicka, M. Łępicka, R. Dobosz, K.J. Kurzydłowski, Biogenic composite filaments based on polylactide and diatomaceous earth for 3D printing, Materials (Basel). 13 (2020) 1–22. https://doi.org/10.3390/ma13204632.
[23] T. Li, H. Sun, B. Wu, H. Han, D. Li, J.-K. Wang, J. Zhang, J. Huang, D. Sun, High-performance polylactic acid composites reinforced by artificially cultured diatom frustules, Mater. Des. 195 (2020) 109003. https://doi.org/10.1016/j.matdes.2020.109003.
[24] S. Lyu, Y. Wang, H. Han, C. Ding, D. Li, J.-K. Wang, J. Zhang, J. Huang, D. Sun, P. Yu, Microstructure characterization and mechanical properties of Al-matrix composites reinforced by artificially-cultured diatom frustules, Mater. Des. 206 (2021) 109755. https://doi.org/10.1016/j.matdes.2021.109755.
[25] I. Zglobicka, A. Chmielewska, E. Topal, K. Kutukova, J. Gluch, P. Krüger, C. Kilroy, W. Swieszkowski, K.J. Kurzydlowski, E. Zschech, 3D Diatom–Designed and Selective Laser Melting (SLM) Manufactured Metallic Structures, Sci. Rep. 9 (2019) 1–9. https://doi.org/10.1038/s41598-019-56434-7.
[26] A. Dubicki, I. Zglobicka, K.J. Kurzydłowskı, Investigation of Energy-Absorbing Properties of a Bio-Inspired Structure, Metals (Basel). 11 (2021) 881.
[27] L. Pfister, C.E. Wetzel, J. Klaus, N. Martínez-Carreras, M. Antonelli, A.J. Teuling, J.J. McDonnell, Terrestrial diatoms as tracers in catchment hydrology: a review, WIREs Water. 4 (2017). https://doi.org/10.1002/wat2.1241.
[28] A. Witkowski, T. Płociński, J. Grzonka, I. Zgłobicka, I. Zgłobicka, M. Bąk, P. Dąbek, A.I.

Gomes, K.J. Kurzydłowski, K.J. Kurzydłowski, Application of Focused Ion Beam Technique in Taxonomy-Oriented Research on Ultrastructure of Diatoms, in: Diatoms Fundam. Appl., 2019: pp. 115–127. https://doi.org/10.1002/9781119370741.ch6.

[29] L. Vásárhelyi, Z. Kónya, Kukovecz, R. Vajtai, Microcomputed tomography–based characterization of advanced materials: a review, Mater. Today Adv. 8 (2020) 1–13. https://doi.org/10.1016/j.mtadv.2020.100084.

[30] I. Zglobicka, Q. Li, J. Gluch, M. Płocińska, T. Noga, R. Dobosz, R. Szoszkiewicz, A. Witkowski, E. Zschech, K.J. Kurzydłowski, Visualization of the internal structure of Didymosphenia geminata frustules using nano X-ray tomography, Sci. Rep. 7 (2017) 1–7. https://doi.org/10.1038/s41598-017-08960-5.

[31] P. Chen, A. Lin, Y. Lin, Y. Seki, A. Stokes, J. Peyras, E. Olevsky, M. Meyers, J. McKittrick, Structure and mechanical properties of selected biological materials, J. Mech. Behav. Biomed. Mater. 1 (2008) 208–226. https://doi.org/10.1016/j.jmbbm.2008.02.003.

[32] A.A. Reka, B. Pavlovski, E. Fazlija, A. Berisha, M. Pacarizi, M. Daghmehchi, C. Sacalis, G. Jovanovski, P. Makreski, A. Oral, Diatomaceous Earth: Characterization, thermal modification, and application, Open Chem. 19 (2021) 451–461. https://doi.org/10.1515/chem-2020-0049.

[33] C.E. Hamm, R. Merkel, O. Springer, P. Jurkojc, C. Maiert, K. Prechtelt, V. Smetacek, Architecture and material properties of diatom shells provide effective mechanical protection, Nature. 421 (2003) 841–843. https://doi.org/10.1038/nature01416.

[34] N. Almqvist, Y. Delamo, B.L. Smith, N.H. Thomson, Å. Bartholdson, R. Lal, M. Brzezinski, P.K. Hansma, Micromechanical and structural properties of a pennate diatom investigated by atomic force microscopy, J. Microsc. 202 (2001) 518–532. https://doi.org/10.1046/j.1365-2818.2001.00887.x.

[35] D. Losic, R.J. Pillar, T. Dilger, J.G. Mitchell, N.H. Voelcker, Atomic force microscopy (AFM) characterisation of the porous silica nanostructure of two centric diatoms, J. Porous Mater. 14 (2007) 61–69. https://doi.org/10.1007/s10934-006-9009-y.

[36] G. Subhash, S. Yao, B. Bellinger, M.R. Gretz, Investigation of mechanical properties of diatom frustules using nanoindentation, J. Nanosci. Nanotechnol. 5 (2005) 50–56. https://doi.org/10.1166/jnn.2005.006.

[37] E. Topal, H. Rajendran, I. Zgłobicka, J. Gluch, Z. Liao, A. Clausner, K.J. Kurzydłowski, E. Zschech, Numerical and experimental study of the mechanical response of diatom frustules, Nanomaterials. 10 (2020) 1–14. https://doi.org/10.3390/nano10050959.

CRediT authorship contribution statement

Izabela Zglobicka: Conceptualization, Methodology, Investigation, Resources, Data Curation, Writing, Visualization, Project administration; **Krzysztof J. Kurzydlowski:** Conceptualization, Methodology, Writing – Review & Editing

Declaration of Competing Interest

☒ The authors declare that they have no known competing financial interests or personal relationships that could have appeared to influence the work reported in this paper.

Graphical abstract